Journal of Geotechnical and Geoenvironmental Engineering. Submitted June 16, 2009; accepted February 2, 2011; posted ahead of print February 3, 2011. doi:10.1061/(ASCE)GT.1943-5606.0000518

PREDICTION AND INTERPRETATION OF THE PERFORMANCE OF A DEEP EXCAVATION IN BERLIN SAND

by

Maria A. Nikolinakou[1,2] S.M.ASCE; Andrew J. Whittle[3], M.ASCE; Stavros Savidis[4] & Ute Schran[5]

ABSTRACT

This paper describes the application of a generalized effective stress soil model, MIT-S1, within a commercial finite element program, for simulating the performance of the support system for the 20m deep excavation of the M1 pit adjacent to the main station "Hauptbahnhof" in Berlin. The M1 pit was excavated underwater and supported by a perimeter diaphragm wall with a single row of prestressed anchors. Parameters for the soil model were based on an extensive program of laboratory tests on the local Berlin Sands. This calibration process highlights the practical difficulties in both measurements of critical state soil properties and in model parameter selection. The predictions of excavation performance are strongly affected by vertical profiles of two key state parameters, the initial earth pressure ratio, K_0, and the in-situ void ratio, e_0. These are estimated from field dynamic penetration test data and geological

[1] Post-doctoral Associate, Civil & Environmental Engineering, Massachusetts Institute of Technology, Cambridge, MA 02139; mariakat@alum.mit.edu.
[2] Now: Research Associate, Bureau of Economic Geology, The University of Texas at Austin, TX 78713.
[3] Department Head, Professor of Civil & Environmental Engineering, Massachusetts Institute of Technology, Cambridge, MA 02139.
[4] Professor & Director, Geotechnical Institute, Technical University of Berlin, Sek. TIB1-B7, Gustav-Meyer-Allee 25, 13355 Berlin, Germany.
[5] CDM Geotechnical Services Division, Cambridge, MA 02139.

Journal of Geotechnical and Geoenvironmental Engineering. Submitted June 16, 2009; accepted February 2, 2011; posted ahead of print February 3, 2011. doi:10.1061/(ASCE)GT.1943-5606.0000518

history. The results show good agreement between computed and measured wall deflections and tie-back forces for three instrumented sections. Much larger wall deflections were measured at a fourth section and may be due to spatial variability in sand properties that has not been considered in the current analyses. The results of this study highlight the importance of basic state parameter information for successful application of advanced soil models.

KEYWORDS: Constitutive model, deformation properties, finite element analysis, diaphragm wall, field instrumentation

Journal of Geotechnical and Geoenvironmental Engineering. Submitted June 16, 2009; accepted February 2, 2011; posted ahead of print February 3, 2011. doi:10.1061/(ASCE)GT.1943-5606.0000518

INTRODUCTION

Although finite element analyses are routinely used in the design of excavation support systems and the interpretation of measured field performance, their predictive accuracy is often quite limited (e.g., Carter et al. 2000). In many cases, the analyses use simplified soil models or lack measurements from which to calibrate model parameters. The geotechnical group at MIT has developed a series of relatively complex elasto-plastic soils (MIT-E3: Whittle & Kavvadas 1994; MIT-S1: Pestana & Whittle 1999) and have demonstrated their application for a number of well-instrumented excavation projects in clays (e.g., Whittle et al. 1993; Hashash &Whittle 1996, 2002; Jen 1997). In each of these projects, the numerical analyses have been supported by site investigation and laboratory testing programs such that model parameters are well-calibrated and the role of the soil model clearly identified.

The current paper follows a similar approach for simulating the performance of a deep excavation in sand: The effective stress-strain-strength properties of the sand are simulated using the MIT-S1 model that has been integrated within the commercial finite element program Plaxis^{TM} (Brinkgreve & Vermeer 2002). The MIT-S1 model incorporates void ratio as a separate state variable (in addition to the state of stress) in order to simulate characteristic transitions from dilative to contractive response associated with increases in the formation void ratio and/or confining stress. The model also uses a new framework for describing the compression behavior of soils, based on the existence of the Limiting Compression Curve, LCC (Pestana & Whittle 1995), which provides the means for unifying the behavior of clays and sands within a single constitutive framework.

Journal of Geotechnical and Geoenvironmental Engineering. Submitted June 16, 2009; accepted February 2, 2011; posted ahead of print February 3, 2011. doi:10.1061/(ASCE)GT.1943-5606.0000518

Model input parameters have been calibrated through an extensive program of laboratory compression and triaxial shear tests on specimens of sand (Glasenapp 2002; Becker 2002) that were obtained from an excavation site in central Berlin (Savidis & Rackwitz 2004). The M1 site is one of a series of excavation pits that were used for underground construction of a new multi-modal transportation corridor through the center of Berlin (collectively referred to as the VZB project - Verkehrsanlagen im Zentralen Bereich). Figure 1 shows that the M1 excavation pit is located to the north of the recently completed Lehrter Bahnhof station (Mönnich & Erdmann 1997). The Berlin Sands were found to be very different from the sands on which MIT-S1 was initially applied. This paper describes the challenges encountered in an independent model calibration for the Berlin Sands, and documents calibration approaches different that those initially established by Pestana (1994; 2002). The model predictions are then compared directly with the field monitoring data, and parametric calculations have been carried out to understand the factors influencing wall deflections and tie-back forces.

The German Society for Geotechnics has used another of the recent excavation projects in Berlin as the basis for a benchmark study to evaluate the accuracy of numerical analyses (Schweiger 2002). In contrast to the current study, the benchmark program provided minimal information on site-specific soil conditions or properties, and found a large scatter in numerical predictions according to the selection of constitutive models and stiffness parameters. Indeed, many of the 17 predictors used the same soil models (such as the elastic-perfectly plastic, Mohr-Coulomb or Hardening Soil, integrated in the Plaxis^{TM} program) but obtained widely varying predictions due to differences in the selection of model parameters. The study highlighted that more refined experimental investigations, including the measurement of stiffness at very small

Journal of Geotechnical and Geoenvironmental Engineering. Submitted June 16, 2009; accepted February 2, 2011; posted ahead of print February 3, 2011. doi:10.1061/(ASCE)GT.1943-5606.0000518

strains, should be employed to provide more reliable data for numerical analysis (Schweiger 2002). The current paper offers such a complementary approach, providing a valuable database on Berlin Sands and building the numerical model from laboratory measurements of the soil properties.

SITE CHARACTERIZATION

The geology of the central area of Berlin is characterized by saturated deposits of quaternary age, reflecting three different glacial periods (Savidis & Rackwitz 2004). The glacial sediments are highly irregular in their horizontal and vertical distributions and also vary widely in their composition, which consists of tills, sands, gravel and boulder clays. The typical vertical profile at the M1 pit, Figure 2b, comprises 3-4m of fill overlying three main sandy till units; 1) S0, upper Holocene sand (approximately 6m with a lower 1m thick organic soil unit, O); 2) S1 glacial sands from the late Pleistocene period (Weichsel glaciation) that are typically 10m thick and 3) S2 glacial sands from the early Pleistocene (Saale glaciation) which are encountered approximately 22m below ground surface. Characteristic engineering properties of these sand units have been reported by GuD/DMT (1994) and Borchert & Richter (1994), based principally on empirical correlations using dynamic probing tests (DPH; after Degebo 1993). These correlations suggest design friction angles, $\phi' = 31^0$, 34^0 and 37.5^0 for the S0, S1 and S2 units, respectively.

The local ground water table is located 2m below the ground surface. Given the high permeability of the surrounding sandy soils (in the range 10^{-3} to 10^{-4} m/s), underwater excavation was considered the only practical construction method, as dewatering would affect a large area,

Journal of Geotechnical and Geoenvironmental Engineering. Submitted June 16, 2009; accepted February 2, 2011; posted ahead of print February 3, 2011. doi:10.1061/(ASCE)GT.1943-5606.0000518

have a significant environmental impact, produce significant settlements, and potentially cause damage to historical buildings etc. (Savidis & Rackwitz 2004). The M1 excavation pit, Figure 2a, is supported by a 1.2-1.5m thick, reinforced-concrete diaphragm wall that extends around the perimeter of the site (approximately 300m long and 25m wide). The wall panels extend to depths ranging from 25m to 31m, corresponding to toe embedments of 6.8m – 7.8m below formation level. The wall is supported by a single row of prestressed tie-back anchors located 2-3m below the ground surface with a spacing ranging between 1.0-1.5m. These are installed with dip angles ranging from 25^0-35^0 and 8m fixed (grouted) anchor lengths within the S1 or S2 sand units (free lengths range from 26-40m). Each tie-back typically uses 8-9 strands of high strength steel tendon (grade 270).

After installing the diaphragm wall and tie-back anchors, excavation is carried out underwater (using a pontoon-mounted crane) to an average final formation grade 20.2m below the initial ground surface. Prior to dewatering, the base of the excavation is sealed by a 1.5m thick underwater concrete slab supported by an array of tension piles. The design for the M1 pit used a system of H-piles installed by a vibratory driver and grouted to ensure good connection with the surrounding sand (RI system). Installation of the RI piles produced significant additional movements of the diaphragm walls. Schran (2003) attributed this behavior in part to the presence of light cementation within the deeper S2 sand unit. The current study focuses of the performance of the support system during the underwater excavation phase, and does not deal directly with subsequent construction of the anchor piles or base slab. The current analyses are also based on properties of reconstituted sands and therefore do not resolve the possible role of cementation on wall movements. The performance of the excavation was monitored through

Journal of Geotechnical and Geoenvironmental Engineering. Submitted June 16, 2009; accepted February 2, 2011; posted ahead of print February 3, 2011. doi:10.1061/(ASCE)GT.1943-5606.0000518

a series of inclinometers installed within the diaphragm walls (Figure 2a) and load cell measurements of forces in the tie-back anchors. Uplift of the base slab was later monitored with horizontal inclinometer tubes (Savidis & Rackwitz 2004; Fig. 2a).

SOIL PROPERTIES AND MODEL PARAMETERS

The effective stress-strain-strength properties for the three sandy till units are modeled using the MIT-S1 model (Pestana & Whittle 1999) under the assumption that all three units have similar material properties but differ principally in their in-situ state (stress conditions, void ratio and stress history). The MIT-S1 formulation is based on the incrementally linearised theory of rate independent elasto-plasticity (e.g., Prévost 1978) and incorporates void ratio as a separate state variable in order to describe peak friction angles and dilation rates as functions of the in-situ void ratio and effective stress state. The main features of the model can be summarized as follows:

1. Large strain shearing is controlled by an isotropic, critical state frictional failure criterion.
2. Shear behavior is described by a single anisotropic bounding surface which is a function of the effective stresses and current void ratio
3. Density hardening of the bounding surface is controlled by the compression behavior of freshly deposited soils represented by the limiting compression curve (LCC; Pestana & Whittle 1995), while rotational hardening accounts for the evolution of anisotropic properties;
4. Small strain non-linearity in shear and stress strain response in unload-reload cycles is described through a perfectly hysteretic formulation.

Journal of Geotechnical and Geoenvironmental Engineering. Submitted June 16, 2009; accepted February 2, 2011; posted ahead of print February 3, 2011. doi:10.1061/(ASCE)GT.1943-5606.0000518

The MIT-S1 model requires 13 material parameters to characterize the behavior of freshly deposited, uncemented clean sands. Pestana et al. (2002) have detailed the selection of these parameters for Toyoura sand, a standard test material whose behavior has been extensively documented in the literature over the last 25 years. For this material, model parameter selection was greatly facilitated by the availability of high quality laboratory test data including high-pressure consolidation tests and extensive programs of triaxial shear tests.

There was no comparable test database available for the Berlin sands and hence, the Authors initiated a laboratory test program on reconstituted test specimens (Glasenapp 2002; Becker 2002). Samples were obtained from the VZB excavation pit (M1) and were blended and mixed to obtain an average set of physical properties, Table 1.

The Berlin sand is a poorly-graded, fine-medium sand with rounded particles (associated with fluvio-glacial deposition). When compared to other natural sands of similar particle size, shape and grading (e.g., Pestana & Whittle 1995) it is apparent that Berlin sand exhibits very low formation void ratios (e_{max} = 0.59 and e_{min} = 0.39) and has a small range of formation conditions (Δe = 0.20, Table 1).

The test program performed by Glasenapp (2002) included a series of four 1-D consolidation tests that were carried to high confining stresses in order to identify parameters associated with the Limiting Compression Curve (LCC) used in the MIT-S1 model. Nineteen triaxial tests were also conducted on specimens formed at void ratios, e_0 = 0.43 – 0.60, that were hydrostatically consolidated to effective stresses, σ'_c = 100, 500 and 800kPa and sheared in both undrained and standard drained compression modes (CIUC and CIDC, respectively). A subsequent program of 16 triaxial shear tests, performed by Becker (2002) (e_0 = 0.43 – 0.57, σ'_c = 100, 800kPa), used

Journal of Geotechnical and Geoenvironmental Engineering. Submitted June 16, 2009; accepted February 2, 2011; posted ahead of print February 3, 2011. doi:10.1061/(ASCE)GT.1943-5606.0000518

more refined testing procedures including reduced-friction end-platens and local strain measurements to enable more reliable interpretation of large-strain, critical state conditions and non-linear stiffness properties at small shear strains.

Table 2 summarizes the input parameters used by the MIT-S1 model together with their physical meaning and the values ultimately selected for Berlin sand. The following paragraphs give further details of the parameter selection:

Compression behavior

The MIT-S1 model assumes that sand specimens compressed from different initial formation densities approach a unique response at high stress levels, referred to as the Limiting Compression Curve (LCC). For 1-D compression tests, the behavior in the LCC regime is characterized by a linear relationship in log[e]-log[σ'_v] space:

$$\log_e(e) = -\rho_c \log_e\left(\frac{\sigma'_v}{\sigma'_{vr}}\right) \tag{1}$$

where ρ_c describes the slope of the LCC curve, and σ'_{vr} is the vertical effective stress at a reference void ratio, e = 1.0.

Figure 3 shows data from four 1-D compression tests on Berlin sand each from a different formation void ratio. The data clearly support the LCC concept, with slope $\rho_c = 0.34$ and $\sigma'_{vr}/p_a = 25.5$, where p_a is the atmospheric pressure. The reference pressure for Berlin sand is substantially smaller than expected from empirical correlations based on mean particle size, d_{50} and angularity. For $d_{50} \approx 0.4$mm, the data compiled by Pestana and Whittle (1995) show σ'_{vr}/p_a increasing from 30 for angular particles (e.g., ground quartz) to 80 for rounded particles (Ottawa sand). This very interesting observation echoes earlier findings of DeBeer (1965) who suggested

Journal of Geotechnical and Geoenvironmental Engineering. Submitted June 16, 2009; accepted February 2, 2011; posted ahead of print February 3, 2011. doi:10.1061/(ASCE)GT.1943-5606.0000518

that the Berlin sands are more sensitive to particle splitting than those of other similar sand deposits (such as Mol sand) and attributed this behavior to impurities in the particles.

The MIT-S1 model assumes that the compressibility parameter, ρ_c, is independent of the lateral earth pressure ratio, σ'_h/σ'_v. However, there is a fixed spacing between the LCC regimes measured in 1-D (K_0-LCC) and hydrostatic (I-LCC) compression. The model (Table 2) actually uses the reference mean effective stress, σ'_r, corresponding to hydrostatic compression as an input parameter. Following Pestana and Whittle (1999) this can be obtained from:

$$\frac{\sigma'_r}{\sigma'_{vr}} = \left(\frac{1+2K_{ONC}}{3}\right)\left(1+\left(\frac{6}{\alpha^2}\right)\left(\frac{1-K_{ONC}}{1+2K_{ONC}}\right)^2\right) \tag{2}$$

where $\alpha^2 = 24\sin^2\phi'_{cs}/(3-\sin^2\phi'_{cs})^2 \le 1$

There are no direct measurements of the earth pressure coefficient for compression of Berlin sand in the high pressure LCC regime. Instead, the current analyses assume $K_{0NC} = 0.5$ which is consistent with empirical correlations (Jaky 1944), assuming a friction angle, $\phi'_{cs} = 31^0$ for shear strength at high confining pressures (Table 2). Substituting into equation 2, $\sigma'_r/\sigma'_{vr} \approx 0.92$ and $\sigma'_r/p_a = 23.5$.

The MIT-S1 model introduces a parameter, θ, to describe the progressive breakage of particles as specimens are compressed. Larger values of θ cause a more gradual transition to the LCC regime, while low values of θ represent materials with well defined yield points associated with particle breakage (typically observed in tests on very uniform materials such as glass ballotini). Figure 3 shows that the measured compression behavior of Berlin sand is well represented by $\theta = 0.25$. This is consistent with expected behavior from empirical correlations

Journal of Geotechnical and Geoenvironmental Engineering. Submitted June 16, 2009; accepted February 2, 2011; posted ahead of print February 3, 2011. doi:10.1061/(ASCE)GT.1943-5606.0000518

between θ and the uniformity coefficient; $\theta \approx 0.1C_u \approx 0.3$ for rounded particles presented by Pestana and Whittle (1995, 1999).

Small strain stiffness properties

The model parameters μ'_0 and C_b define the elastic Poisson's ratio and bulk modulus that control the stiffness of sand immediately upon load reversal (Pestana, 1994):

$$C_b = \frac{K_{\max}}{p_a}\left(\frac{e}{1+e}\right)\left(\frac{\sigma'}{p_a}\right)^{-1/3} \tag{3a}$$

where e is the void ratio, σ' the mean effective stress and K_{max} the small strain elastic bulk modulus. The small strain elastic shear modulus, G_{max} can then be derived from C_b and μ'_0:

$$\frac{2G_{\max}}{K_{\max}} = \frac{3(1-2\mu'_0)}{1+\mu'_0} \tag{3b}$$

The model parameters C_b and μ'_0 have been derived from local strain measurements in the triaxial shear tests performed by Becker (2002).

The tangential elastic moduli (and hence Poisson's ratio during unloading) are updated as a function of stress variations and a parameter, ω. This parameter captures the non-linearity in the effective stress paths during unloading (ω =0 would yield a linear relationship between K_0 and OCR). In principle, ω can be interpreted from the unloading effective stress path in a rigid-walled, 1-D compression device (requiring very precise measurements of lateral stresses) or though very accurate small strain measurements in both vertical and radial directions during unloading in a triaxial cell. No such measurements were carried out for Berlin sand, and instead ω = 1.0 was selected based on recommendations of Pestana, from typical data reported in the

Journal of Geotechnical and Geoenvironmental Engineering. Submitted June 16, 2009; accepted February 2, 2011; posted ahead of print February 3, 2011. doi:10.1061/(ASCE)GT.1943-5606.0000518

literature (Pestana et al. 2005). This value yields non-linearity in the effective stress path even for OCR≈1.5. Non-linear behavior at relatively small shear strain levels (less than 0.1%) is controlled by a second parameter ω_s which in principle can be fitted to local strain data on modulus degradation.

Shear Behavior

In the prior formulation of MIT-S1 for Toyoura sand, Pestana et al. (2002) tried to develop procedures that can provide unambiguous estimation of the remaining six model input parameters as follows: 1) the large strain friction angle, ϕ'_{cs}, measured in either drained or undrained shear tests; 2) the peak friction angle measured in drained shear tests on dense specimens (to enable selection of parameters ϕ'_{mr}, p; Table 2); 3) the effective stress paths in undrained shearing enable selection of parameters m and ψ, and 4) the small strain non-linear stiffness are used to define ω_s. This approach also minimizes the need to measure critical state conditions in the laboratory tests.

For Berlin sand it has proved difficult to follow such a simple procedure due to uncertainties in the critical state and variability in the peak friction angles as shown in Figures 4, 5 and 6:

Figure 4 shows typical drained shear tests on the Berlin sand at three different confining pressures (and formation void ratio, e_0 = 0.51). As expected, the measured peak friction angle decreases with the level of confining pressure and the three tests converge to a unique stress ratio at large shear strains, corresponding to a friction angle of approximately 31^0. This is assumed to be the critical state friction angle in the MIT-S1 model (ϕ'_{cs}, Table 2), although it is not clear

Journal of Geotechnical and Geoenvironmental Engineering. Submitted June 16, 2009; accepted February 2, 2011; posted ahead of print February 3, 2011. doi:10.1061/(ASCE)GT.1943-5606.0000518

from the volumetric strain data if the samples have actually achieved critical state conditions (zero rate of volumetric strain) at the end of each test (with shear strains exceeding 20%).

There is a relatively small range in peak friction angles measured in the CIDC shear tests, Figure 5 ($\phi'_{peak} = 32^0 - 40^0$), and significant variability (up to 2^0) between tests performed under nominally identical formation conditions. The peak friction angles are lower than would be expected for other quartzitic sands (at a similar range of confining pressures and void ratios) as noted by DeBeer (1965). Preliminary estimates indicated that the observed maximum friction angles can be simulated by combinations of two model input parameters, $p = 2$ - 3 and $\phi'_{mr} = 8^0$ - 16^0. Although values for p were consistent with prior data for other quartzitic sands, the range for ϕ'_{mr} is much lower than expected from prior studies (e.g., Pestana et al. 2002).

The MIT-S1 model assumes that there is a unique critical state condition for homogeneous shearing to large strains in the triaxial compression shear mode. The critical state in triaxial modes of shearing can be estimated in closed-form (see Pestana et al. 2005) as a function of the three input parameters, p, ϕ'_{mr} and m (i.e., the same parameters affecting predictions of the peak friction angle). In practice, critical state conditions are rarely achieved in laboratory shear tests on sands. Shear banding or strain localization commonly occurs in drained shear tests (where post peak strain softening occurs concurrently with dilative volumetric strains), while undrained shear tests often cavitate before reaching a steady state of deformation. Testing on Berlin sand was no exception to this, as can be seen in Figure 6. The figure provides a symbolic interpretation of the end points measured in the triaxial shear tests. The arrowhead directions indicate the proximity of the critical state in each test based on a subjective interpretation of the data. The size of these symbols gives an indication of test quality. The results show a broad band

Journal of Geotechnical and Geoenvironmental Engineering. Submitted June 16, 2009; accepted February 2, 2011; posted ahead of print February 3, 2011. doi:10.1061/(ASCE)GT.1943-5606.0000518

of possible locations for the critical state line defined from combinations of drained tests that either contract or dilate towards critical state, and undrained tests that generate positive or negative shear induced pore pressures.

Figure 6 also illustrates the role of the model input parameters in predictions of the critical state for Berlin sand. The parameter m controls the location of the critical state at high pressures (nominally for $\sigma' > 1$MPa), while p and ϕ'_{mr} both affect predictions in the lower stress range. The final parameter set reported in Table 2 ($p = 2.7$, $m = 0.42$ and $\phi'_{mr} = 12.5^0$) provided the most consistent prediction of both the critical state conditions and peak friction angles in CIDC shear tests, as shown in Figure 5. The model tends to underestimate the measured peak friction angles at low confining pressures ($\sigma'_c = 100$kPa) but is in good agreement with data for $\sigma'_c =$ 500, 800kPa. The computed critical state line has a critical void ratio $e_{crit} = 0.6$ (i.e., $e_{crit} \approx e_{max}$) at low effective stress (Fig. 6). According to Ishihara (1993), sands with a state index I_s (=[$e_{crit} - e$]/[e_{crit}-e_{cs}]) < 0 will collapse during undrained shearing with zero residual strength.

The final model input parameter, ψ, controls rotational hardening of the yield surface in MIT-S1 and hence, characterizes the evolution of anisotropic deformation and strength properties. In prior studies, ψ has been calibrated from the stress-strain response measured during undrained shearing to large strains. For example, Figure 7 illustrates the selection of ψ for one undrained shear test. The parameter has minimal effect on the predicted response until the mobilized friction exceeds ϕ'_{cs}. For the Berlin sand, there is a strong cross-coupled effect of ψ with ω_s (not previously found for Toyoura sand). Figure 8 shows that ω_s has a very similar effect as ψ on the undrained stress-strain response at large shear strains and also influences the initial effective stress path.

Journal of Geotechnical and Geoenvironmental Engineering. Submitted June 16, 2009; accepted February 2, 2011; posted ahead of print February 3, 2011. doi:10.1061/(ASCE)GT.1943-5606.0000518

Figure 9 compares model predictions for $\psi = 10$ and 25 with the measured shear stress-strain behavior from CIDC tests on Berlin sand consolidated to σ'_c = 800kPa from different formation void ratios. Although the results show that the model tends to underestimate the initial shear stiffness and peak shear resistance of the densest specimens (i.e., e_0 = 0.462, 0.491), the general trends in behavior are well described by the model with $\psi = 10$ (and other input parameters listed in Table 2).

INITIAL SOIL STATE PARAMETERS

In order to apply MIT-S1 for simulations of excavation performance for the M1 pit, it is first necessary to establish ranges of two key state variables, e_0, the in-situ void ratio and K_0 the lateral earth pressure coefficient at rest. There are no direct measurements of these parameters. The only in-situ data are from Dynamic Probing (DPH) tests performed in conjunction with the boreholes shown in Figure 2a. The DPH N_{10} blowcount data can be correlated with relative density, D_r:

$$D_r = 0.23 + 0.38 \log_e (N_{10}) \tag{4}$$

Equation 4 follows DIN 4094-3 and uses the laboratory values of e_{max} and e_{min} for Berlin Sands (Table 1). Figure 10 summarizes the resulting profiles of estimated void ratio from 4 typical locations around the M1 pit (Fig. 2a). Although the results do show a trend of increased density with depth, there is considerable scatter in estimated void ratio at any selected depth. The data suggest that the upper sand unit, S0 is in loose state with $e_0 \approx 0.6$ (upper 8m), while the lowest unit, S2 is very dense with $e_0 \approx 0.3 - 0.4$; the intermediate S1 unit has $e_0 \approx 0.5 - 0.6$. The

Journal of Geotechnical and Geoenvironmental Engineering. Submitted June 16, 2009; accepted February 2, 2011; posted ahead of print February 3, 2011. doi:10.1061/(ASCE)GT.1943-5606.0000518

Authors have not found any clear spatial pattern in the data and hence, assume the same void ratio profile in analyses at each of the instrumented sections.

The in-situ K_0 values should be strongly influenced by the geological history. In principle, the heavily pre-compressed Pleistocene units (S1 and S2) can be expected to have higher values of K_0 than the recent Holocene unit, S0. Based on this reasoning (and in the absence of any direct measurements), the Authors have assumed default values, K_0 = 0.5 and 1.0 for S0 and S1/S2 units, respectively.

An alternative method for estimating the void ratio is through the empirical correlations used for the mobilized friction angles in each of the three sand units. According to GuD/DMT (1994), ϕ' = 31^0, 34^0 and 37.5^0 for the S0, S1 and S2 units, respectively. Assuming that these friction angles are to be correctly represented by the MIT-S1 model, then a consistent set of in-situ void ratios can be obtained from the model predictions relating peak friction to void ratio and effective confining stress (cf. Fig. 5). This procedure is illustrated in Figure 11. The soil profile is approximated by the three sand units (ignoring secondary details such as the fill and organic layers), Figure 11a. For the upper S0 sand, $\phi' = \phi'_{cs}$ and hence, $e_0 \geq 0.6$. For S1, the in-situ stress ranges from 135 – 265 kPa and hence, e_0 = 0.51 – 0.53, is consistent with ϕ' = 34°. By a similar procedure e_0 = 0.40 – 0.45 in S2. These results suggest higher in-situ void ratios than those derived directly from DPH correlations (Fig. 10).

The MIT-S1 model simulates non-linear stress-strain behavior from small levels of shear strain. Figure 12 illustrates the profile of the small strain shear modulus, G_{max}, computed for the M1 site based on laboratory stiffness parameters and the assumed profiles for K_0 and e_0 (eqns. 3a, 3b; Table 2). These results are in very good agreement with well-known empirical

Journal of Geotechnical and Geoenvironmental Engineering. Submitted June 16, 2009; accepted February 2, 2011; posted ahead of print February 3, 2011. doi:10.1061/(ASCE)GT.1943-5606.0000518

correlations for G_{max} of sands such as those proposed by Hardin & Richart (1963), which are also included in the recommendations of the German Society for Geotechnical Engineering (DGGT). In principle these results should match closely the values of G_{max} from measurements of cross-hole shear wave velocity (v_s) reported in preliminary site investigation work by GuD-DMT (1994). However, Figure 12 shows that the cross-hole G_{max} data are much lower than expected. Indeed, the cross-hole values of G_{max} are actually lower than empirical estimates of 'reload modulus' used in the original wall design methods for the VZB pits. The source of this discrepancy is not known but it is important to note that the small strain stiffness used by MIT-S1 is higher than the modulus values from prior empirical correlations in Berlin.

NUMERICAL MODEL FOR M1 EXCAVATION

Two dimensional finite element analyses of the M1 excavation pit have been carried out using the commercial finite element code, Plaxis^{TM} (Brinkgreve & Vermeer 2002). The MIT-S1 model was integrated within this code through a 'user-defined' constitutive model interface. The analyses focus on 4 half-sections through the excavation pit (all similar to Fig. 2b) that correspond to the locations of inclinometers MQ2 – MQ5 (Fig. 2a). The characteristics of the cross sections are summarized in Table 3. It should also be noted that the ground surface on the West side of the M1 pit is 1.5m lower than the East side and that the excavation progressed northwards, with the final depth in MQ2 reached more than a month after MQ4. The soil is represented by 6-node plane strain elements, the tie-backs by using a combination of node-to-node anchor and 'geotextile' elements (for the free and fixed anchor length, respectively) and the diaphragm wall by using elastic Mindlin-beam elements. The analyses assume that the wall is

Journal of Geotechnical and Geoenvironmental Engineering. Submitted June 16, 2009; accepted February 2, 2011; posted ahead of print February 3, 2011. doi:10.1061/(ASCE)GT.1943-5606.0000518

'wished-in-place' and hence, does not consider local changes in stresses or soil properties associated with trench excavation and concreting. The analyses simulate the initial excavation to El. 30.5m, followed by tie-back installation and prestress, then by four stages of underwater excavation to the final formation level (no quantitative data on the underwater excavation stages were available).

Results

Initial parametric analyses were carried out assuming a uniform soil profile (single sand unit) at a reference section, MQ3, to investigate the effects of the in-situ state parameters e_0 and K_0. Figure 13 summarizes the measured wall deflections and tie-back loads immediately after prestress and at final formation stage. The measured data are compared with finite element simulations for a constant void ratio (e_0 = 0.5) and three possible values of K_0 = 0.5, 0.75 and 1.0. The results show that higher K_0 values generate larger wall deflections and anchor loads at the end of excavation. The measured data lie within the mid-range of the computed maximum wall deflections (1.5cm to 2.8cm) while the tie-back force is in close agreement with results for K_0 = 1.0. However, the analyses generally underestimate the wall pull-back upon initial application of the prestress and overestimate deflections at the top of the wall during excavation.

Figure 14 shows a further set of calculations for a constant K_0 (= 0.5) and three possible values of e_0 = 0.4, 0.5 and 0.6. The in-situ void ratio has minimal effect on wall deflections at prestress or on values of the tie-back force at the end of excavation. However, wall deflections during excavation are very strongly influenced by e_0. The maximum wall deflection increases from 1.0cm to 4.0cm as e_0 increases from 0.4 to 0.6. Movements at the top and toe of the wall

Journal of Geotechnical and Geoenvironmental Engineering. Submitted June 16, 2009; accepted February 2, 2011; posted ahead of print February 3, 2011. doi:10.1061/(ASCE)GT.1943-5606.0000518

are little affected by changes in e_0 between 0.4 and 0.5 and are generally in close agreement with the measured data.

The parametric analyses highlight the need to sub-divide the vertical profile and corroborate the variation of state variables discussed above. A third set of analyses for MQ3, Figure 15, consider a more realistic profile represented by three sand units with e_0 = 0.60, 0.53 and 0.40 and K_0 = 0.5, 1.0 and 1.0 in S0, S1 and S2, respectively. The overall pattern of predictions is much improved for this case. The numerical analyses are in excellent agreement with the movements at the top and toe of the wall at the final formation grade but underestimate the maximum wall deflection by 0.5cm. Bending of the wall is much better described than in either of the two preceding sets of analyses with homogeneous state variables. It is also interesting to note that the model predicts very small surface settlements (up to 0.2cm) in the retained soil, and 1.5cm of heave below the base of excavation. Unfortunately there are no data to evaluate these results.

Figures 16, 17 and 18 summarize further computations and measurements for three independent cross-sections (MQ5, MQ4 and MQ2, respectively, cf. Fig. 2a). Table 3 summarizes the differences in support systems and excavation depths for each of these sections.

Section MQ5, Figure 16, is immediately opposite MQ3 but is supported with a thinner diaphragm wall section (1.2m vs. 1.5m), less steeply inclined anchor (25^0 vs. 35^0 dip angle) and lower prestress load. The measured data show slightly higher maximum wall deflections (2.7cm vs. 2.1cm at MQ3) and movements at the top of wall (1.1cm vs. -0.2cm at MQ3) that are consistent with these differences in support conditions. The measured toe movements are almost the same at both MQ3 and MQ5 (0.3cm).

Journal of Geotechnical and Geoenvironmental Engineering. Submitted June 16, 2009; accepted February 2, 2011; posted ahead of print February 3, 2011. doi:10.1061/(ASCE)GT.1943-5606.0000518

For this section, the numerical predictions are in excellent agreement with the measured (top, toe and maximum) wall deflections and anchor forces at the final formation level. The analyses also predict much larger settlements at MQ5 (1.2cm vs. 0.2cm for MQ3) due to differences in anchor location and prestress, while predictions of heave inside the excavation are almost the same for both MQ5 and MQ3.

Section MQ4, Figure 17, uses the same diaphragm wall section as MQ5 but has shallower dip of the tie-back anchors and is designed with lower anchor stiffness and prestress (Table 3). The excavation is also 1.8m shallower at MQ4. Numerical predictions for MQ4 are consistent with expected behavior based on these perturbations of support conditions. The computed maximum wall deflection (1.9cm) is smaller than that found at MQ5 (2.5cm), while computed movements at the top of the wall are larger (2.0cm vs 1.2cm for MQ5). Although there is excellent agreement between the computed and measured top-of-wall deflection and anchor load, the numerical analysis underestimates significantly the measured toe movement (0.2cm vs. 0.9cm) and hence, underestimates the measured maximum wall deflection (2.6cm). These discrepancies are not easily explained from results at the prior sections MQ5 or MQ3. Although the borehole data do indicate a thicker zone of organic materials in the vicinity of MQ4, there is no evidence to suggest high void ratios in the sands from DPH soundings at B1129 (cf. Figs. 2a, 10). However, there were construction problems associated with diaphragm wall panel installation in this area (using a hydrofraise), and it is possible that this may be associated with local loosening of the soil at the toe of the wall.

Finally, results for MQ2 in Figure 18 are most directly comparable to conditions at the reference section MQ3 (Fig. 15). These two use the same diaphragm wall section (1.5m) and

Journal of Geotechnical and Geoenvironmental Engineering. Submitted June 16, 2009; accepted February 2, 2011; posted ahead of print February 3, 2011. doi:10.1061/(ASCE)GT.1943-5606.0000518

have similar anchor inclination (38^0 vs 35^0 for MQ3), but the excavation is almost 2m deeper at MQ2. The wall deflection data from MQ2 differ significantly from any of the three preceding sections. It is the only section where there are significant inward wall deflections measured at the prestress stage (up to 0.7cm at mid-depth of the wall). At the end of excavation the maximum measured wall deflection is approximately 5.2cm (vs 2.1cm at MQ3). This difference in measured performance is certainly not expected from the variations in support conditions (but could still be related to unreported variations in construction activities). The numerical analyses predict maximum wall deflections up to 2.4cm, of which 0.7cm occurs at the top of the wall (vs. 2.3cm measured), while there is good agreement at the toe (0.3cm). The predictions are consistent with the other three sections and hence, the underestimation of wall deflections is again most likely related to spatial variability in soil properties. In this case, the data appear to reflect lower density (higher void ratio) in the S0 and S1 units and/or higher K_0 in the upper S0 unit. However, there is again no indication of such variability from the local DPH data (B1137, Fig. 10).

DISCUSSION

The preceding numerical analyses have shown that it is possible to obtain reasonable predictions of wall deflections and tie-back forces using a constitutive model that is calibrated to results of laboratory tests on reconstituted sand specimens. The MIT-S1 model is able to describe realistically variations in the shear strength and stiffness parameters measured at

Journal of Geotechnical and Geoenvironmental Engineering. Submitted June 16, 2009; accepted February 2, 2011; posted ahead of print February 3, 2011. doi:10.1061/(ASCE)GT.1943-5606.0000518

different confining stresses and void ratios using a single set of input parameters. However, further judgment has been needed in the selection of in-situ state variables, e_0 and K_0.

It is certainly plausible to achieve comparable agreement between computed and measured behavior using simpler constitutive soil models. Here the difficulty lies in the rational selection of input parameters. None of the 'simple models' used in current practice can describe the full range of stiffness and shear strength properties measured in the laboratory tests on Berlin sand. Instead, it is more effective to consider optimizing the selection of key input parameters for these models and then comparing the optimized parameters with results of the laboratory tests. For example, the Authors have optimized the selection of shear strength and stiffness parameters for the Hardening Soil model (Schanz et al. 2000) within the Plaxis^{TM} program at section MQ3. This has been accomplished using genetic algorithms similar to those described by Levasseur et al. (2008) and optimizing the selection of two model input parameters (E_{50}^{ref} and ϕ'_{peak}). The objective function was set to minimize differences in the computed and measured tie-back forces and lateral wall deflections (over the full depth of the wall) at the preload stage and at the end of excavation. Table 4 summarizes the input for the Hardening Model, including the selected range for the optimizing parameters. Figure 19 plots the predictions obtained by the best-fit Hardening Soil model parameters at MQ3. There is good agreement between the computed and measured maximum wall deflections at the end of excavation. However, the model overestimates inward movements at the toe of the wall and, compared to the MIT-S1 predictions, yields larger deformations below the base of excavation. Moreover, it predicts heave behind the wall, an improbable response for the retained soil. The benchmark study on a similar Berlin excavation (Schweiger 2002) also reports heave predictions, illustrating the inadequacy of some of the

Journal of Geotechnical and Geoenvironmental Engineering. Submitted June 16, 2009; accepted February 2, 2011; posted ahead of print February 3, 2011. doi:10.1061/(ASCE)GT.1943-5606.0000518

models used and the lack of calibration data for the Berlin Sands. The backfitted value for the peak angle, $\phi'_{peak} = 36.6^0$ is in reasonable agreement with the friction angle measured at σ'_c = 100kPa (test #570, Fig. 4). The predicted dilation angle, $\psi_d = 6.8^0$ is at the upper limit of dilation angles measured in the laboratory triaxial tests (cf., #570, Fig. 4). However the elastic moduli, E_{50} = 45 - 128 MPa (for σ'_c = 100 - 800kPa) are significantly lower than the stiffness values measured in the corresponding test ($E_{50} \approx$ 140 - 245 MPa respectively). These results suggest the need for further refinement in the selection of HS model parameters for the lower sand unit S2, but give no insight into the broader applicability of the laboratory test results.

CONCLUSIONS

This paper has described the application of a generalized effective stress soil model, MIT-S1, for predicting the performance of deep excavations in Berlin sand. The model was calibrated using data from an extensive laboratory program of tests on reconstituted sand specimens. The calibration process proved quite challenging due to variability in the peak friction with small perturbations in formation void ratio, and uncertainties in the interpretation of critical state conditions.

The model has been used in finite element simulations of the underwater excavations at a series of instrumented sections in the M1 pit near to the Lehrter Bahnhof in central Berlin. Site investigations for this project showed that the vertical profile comprised three main sand units, while in-situ density and shear strength were estimated using correlations to DPH N_{10} blowcount data. The measured data show significant variability in the estimated in-situ void ratio. The current study has assumed a single average profile and used the DPH correlations and

Journal of Geotechnical and Geoenvironmental Engineering. Submitted June 16, 2009; accepted February 2, 2011; posted ahead of print February 3, 2011. doi:10.1061/(ASCE)GT.1943-5606.0000518

background information on the geological history to estimate the in-situ void ratio, e_0, and earth pressure coefficients, K_0.

The numerical simulations are in very good agreement with measured diaphragm wall deflections and forces in the single row of tie-back anchors for three of the four instrumented sections considered in this study. The measured data for a fourth section (MQ2) show much larger wall movements than predicted (or expected based on the design of the lateral earth support system), while unusual wall-toe movements occurred at a second section (MQ4). Although these deviations in behavior are most probably caused by spatial variations in soil properties, there is no supporting evidence from the local DPH data.

The study shows that realistic predictions of excavation performance can be achieved through careful site-specific calibration of sand behavior using a constitutive model that is able to represent variations in stress-strain-strength properties as functions of the confining stress and void ratio. This approach provides a more consistent method of model validation than generic benchmark studies using aggregated soil properties. However, further work is needed to address effects of spatial variability in site-specific applications.

ACKNOWLEDGEMENTS

This research was supported by collaboration grants from the NSF Western Europe program (INT-0089508) and DAAD. The laboratory tests were performed at the MIT geotechnical laboratory under the expert supervision of Dr John Germaine. Special thanks to Ralf Glasenapp and Tim Becker for their meticulous experimental work, to Dr Frank Rackwitz for his help in

Journal of Geotechnical and Geoenvironmental Engineering. Submitted June 16, 2009; accepted February 2, 2011; posted ahead of print February 3, 2011. doi:10.1061/(ASCE)GT.1943-5606.0000518

compiling the field data, to Gonzalo Corral for performing the inverse analyses in Plaxis™, and to the reviewers for improving the original manuscript.

REFERENCES

Becker, T. (2002). "Triaxialversuche mit reduzierter Endflächenreibung zur Untersuchung des Materialverhaltens von Berliner Sand," Diploma thesis, Technical University of Berlin, Germany (in German, Figure captions also in English).

Borchert, K.M., and Richter, T. (1994). "Gutachterliche Beurteilung zum Ansatz der Bodensteifigkeiten beim Bauvorhaben VZB-Berlin", *GuD Consult*, Berlin, Germany (in German).

Brinkgreve, R.B.J., and Vermeer, P.A. (2002). PLAXIS: Finite Element Code for Soil and Rock Analyses, Version 8, Balkema.

Carter, J.P., Desai, C.S., Potts, D.M., Schweiger, H.F., and S.W. Sloan (2000). "Computing and Computer Modelling in Geotechnical Engineering," *Proc. GeoEng2000*, Melbourne, Technomic Publishing, Lancaster, 1, 1157-1252.

De Beer, E.E. (1965). "Influence of the mean normal stress on the shearing strength of sand," *Proc. 6th ICSMFE*, Montreal, 1, 165-169.

Degebo - Deutsche Forschungsgesellschaft für Bodenmechanik (1993). "Gutachten über die Untergrundverhältnisse in der Trasse der geplanten Nord-Süd-Verbindung zwischen Paul-Löbe-Straße und dem Rampenbauwerk auf dem Gelände des Hamburg-Lehrter-Gueterbahnhofes in Berlin-Tiergarten"; Gutachten im Auftrag der Deutschen Reichsbahn; Auftragsnummer 12.000/07; Berlin, 30.12.1993 (in German).

Journal of Geotechnical and Geoenvironmental Engineering. Submitted June 16, 2009; accepted February 2, 2011; posted ahead of print February 3, 2011. doi:10.1061/(ASCE)GT.1943-5606.0000518

Glasenapp, R. (2002). "Triaxialversuche mit Berliner Sand," Diploma thesis, Technical University of Berlin, Germany (in German, Figure captions also in English).

GuD/DMT Arbeitsgemeinschaft Umweltgeologie und Geotechnik (1994). "Zusammenfassender Bericht Baugrund - Altlasten - Alte unterirdische Bauwerke"; Gutachten im Auftrag der Deutschen Reichsbahn und der Senatsverwaltung für Bau- und Wohnungswesen; Berlin (in German).

Hardin, B.O., and Richart, Jr., F., E. (1963). "Elastic wave velocities in granular soils", *Journal of Soil Mechanics and Foundations Division*, ASCE 89(SM1), 33-65.

Hashash, Y.M.A., and Whittle, A.J. (1996). "Ground movement prediction for deep excavations in soft clay," *Journal of Geotechnical & Geoenvironmental Engineering*, ASCE, 122(6): 474-486.

Hashash, Y.M.A., and Whittle, A.J. (2002). "Mechanisms of Load Transfer and Arching for Braced Excavations in Clay," *Journal of Geotechnical & Geoenvironmental Engineering*, ASCE, 128(3): 187-197.

Ishihara, K. (1993). "Liquefaction and flow failure during earthquakes," *Géotechnique*, 43(3), 351-415.

Jaky, J. (1944). "The coefficient of earth pressure at rest", J. Soc. Eng. Arch. (Magyar Mernok es Epitesz-Egylet Kozlonye; in Hungarian), 355-358

Jen L. (1997). "The design and performance of deep excavations in clay", Ph.D Thesis, Massachusetts Institute of Technology, Cambridge, USA

Journal of Geotechnical and Geoenvironmental Engineering. Submitted June 16, 2009; accepted February 2, 2011; posted ahead of print February 3, 2011. doi:10.1061/(ASCE)GT.1943-5606.0000518

Levasseur, S., Malecot, Y., Boulon, M. and Flavigny, E. (2008). "Soil parameter identification using a genetic algorithm," *International Journal for Numerical and Analytical Methods in Geomechanics,* 32, 189-213.

Mönnich, K.D., and Erdmann, J. (1997). "Planning New Public Transportation in Berlin", *Structural Engineering International*, 4, 231-232.

Pestana J.M. (1994). "A unified constitutive model for clays and sands", Sc.D thesis, Massachusetts Institute of Technology, Cambridge, MA.

Pestana, J.M., and Whittle, A.J. (1995). "Compression model for cohesionless soils," *Géotechnique*, 45(4), 611-633.

Pestana, J.M., and Whittle A.J. (1999). "Formulation of a unified constitutive model for clays and sands," *International Journal for Numerical and Analytical Methods in Geomechanics*, 23, 1215-1243.

Pestana, J.M., Whittle, A.J., and Salvati, L. (2002). "Evaluation of a constitutive model for clays and sands: Part I – Sand behavior," *International Journal for Numerical and Analytical Methods in Geomechanics*, 26, 1097-1121.

Pestana, J.M., Nikolinakou, M.A., and Whittle, A.J. (2005): "Selection of material parameters for sands using the MIT-S1 model," *Soil Constitutive Models: Evaluation, Selection and Calibrtion,* ASCE, GSP 128, 425-439.

Prévost J. H. (1978). "Plasticity theory for soil stress-strain behavior*," Journal of Engineering Mechanics Division,* ASCE, 104 (5), 1177-1194.

Rackwitz F. (2003). "Numerische Untersuchungen zum Tragverhalten von Zugpfählen und Zugpfahlgruppen in Sand auf der Grundlage von Probebelastungen", Ph.D thesis, Technical University of Berlin, Germany (in German, Figure captions also in English).

Savidis S.A., and Rackwitz F. (2004). "Geotechnical and Environmental Consideration by Planning and Construction of the Transportation Infrastructure in the Centre of Berlin", *Proc., 5th Intl Conf. on Case Histories in Geotechnical Engineering*, New York, NY, paper 5.32.

Schanz, T., Vermeer, P.A. & Bonnier, P.G. (1999). "The Hardening Soil model: Formulation and verification," *Beyond 2000 in Computational Geotechnics*, Balkema, Rotterdam, 16p.

Schran U. (2003). "Untersuchungen zu Verschiebungen von Schlitzwänden beim Unterwasseraushub in Berliner Sanden," Ph.D thesis, Technical University of Berlin, Germany (in German)

Schweiger, H.F. (2002). "Benchmarking in Geotechnics. Part 1: Results for benchmarking; Part 2: Reference solution and parametric study", Institute for Soil Mechanics and Foundation Engineering, Graz University of Technology, Austria.

Whittle A. J., and Kavvadas M. (1994). "Formulation of the MIT-E3 constitutive model for overconsolidated clays," *Journal of Geotechnical Engineering*, ASCE, 120(1), 173-198.

Whittle A.J., Hashash Y.M.A., and Whitman, R.V. (1993), "Analysis of deep excavation in Boston", *Journal of Geotechnical Engineering*, ASCE, 119(1), 69-90.

Journal of Geotechnical and Geoenvironmental Engineering. Submitted June 16, 2009; accepted February 2, 2011; posted ahead of print February 3, 2011. doi:10.1061/(ASCE)GT.1943-5606.0000518

Table 1: Physical properties of Berlin sand

Property	Test Material	Avg. Lehrter Bahnhof[1]
Mineralogy	Quartz & Feldspar	
Grain shape	Rounded	
Specific gravity of solids, G_s	2.65	
Mean particle size, d_{50} (mm)	0.38	0.42
Coefficient of uniformity, C_u (= d_{60}/d_{10})	3.0	3.1
Coefficient of curvature, C_z (= $d_{30}^2/d_{10}d_{60}$)	1.2	--
Maximum void ratio[2], e_{max}	0.590	0.59
Minimum void ratio[2], e_{min}	0.389	0.40
Range of formation void ratios, Δe	0.201	0.19

[1] Test data reported by Rackwitz (2003)

[2] Tests performed according to DIN 18124 (1997)

Journal of Geotechnical and Geoenvironmental Engineering. Submitted June 16, 2009; accepted February 2, 2011; posted ahead of print February 3, 2011. doi:10.1061/(ASCE)GT.1943-5606.0000518

Table 2: Input parameters for the MIT-S1 model

Parameter / Symbol	Physical contribution /meaning	Berlin Sand
ρ_c	Compressibility of sands at large stresses (LCC regime)	0.34
σ'_r/p_a	Reference stress at unit void ratio for conditions of hydrostatic compression in the LCC regime	23.5
θ	Describes first loading curve in the transitional stress regime	0.25
h	Irrecoverable plastic strain, OC[1]	-
K_{0NC}	K_0 in the LCC regime	0.50
μ'_0	Poisson's ratio at load reversal	0.28
ω	Non-linear Poisson's ratio. 1-D unloading stress path	1.00
ϕ'_{cs}	Critical state friction angle in triaxial compression	31.0^0
ϕ'_{mr} p	Control the maximum friction angle as a function of formation density (at low effective stresses)	12.5^0 2.7
m	Controls the cap geometry of the bounding surface	0.42
ω_s	Small strain (< 0.1%) non-linearity in shear	4.0
ψ	Rate of evolution of anisotropy. Stress-strain curves	10
C_b	Small strain stiffness at load reversal	950

[1] Parameter not needed in current study

Journal of Geotechnical and Geoenvironmental Engineering. Submitted June 16, 2009; accepted February 2, 2011; posted ahead of print February 3, 2011. doi:10.1061/(ASCE)GT.1943-5606.0000518

Table 3: Properties of excavation support structures at inclinometer locations

		Wall		Tieback Anchors					
Location	Excav. Depth (m)	Thickness (m)	Height (m)	Spacing (m)	Free Length (m)	Dip Angle (^{0})	No. Tendons	A_s (cm^2/m)	Pre-stress (kN/m)
MQ2	23.30	1.5	31.05	1.0	40.0	38	10	18.15	400
MQ3	21.40	1.5	28.70	1.0	34.5	35	8	14.52	540
MQ4	18.00	1.2	24.80	1.5	30.5	19	8	9.68	213
MQ5	20.10	1.2	27.20	1.2	26.5	25	9	13.61	292

Note:

Wall: Elastic properties, E = 30GPa, ν = 0.15, γ_c = 24kN/m^3

Tiebacks: Head at El. +31m; fixed anchor length, L_2 = 8.0m

15.2 mm diameter steel tendons, modulus, E = 210GPa

Journal of Geotechnical and Geoenvironmental Engineering. Submitted June 16, 2009; accepted February 2, 2011; posted ahead of print February 3, 2011. doi:10.1061/(ASCE)GT.1943-5606.0000518

Table 4: Input parameters used in the generic algorithms for the Hardening Soil Model

E_{50}^{ref} **(MPA)**	E_{oed}^{ref} (MPA)	E_{ur}^{ref} (MPA)	ν_{ur}	m	p_{ref} (kPA)	ϕ'_{peak} (^{0})	ψ'_d (^{0})
[20 to 200]	$b\,E_{50}^{ref}$	$3\,E_{50}^{ref}$	0.25	0.5	100	**[30 to 40]**	calculated

Notes:

In Plaxis^{TM}, the following relations are used to calculate E_{50} and dilation angle ψ'_d :

$$E_{50} = E_{50}^{ref}\left(\frac{\sigma'_c}{p_{ref}}\right)^m \quad ; \quad \sin\psi'_d = \frac{(\sin\phi'_{peak} - \sin\phi'_{cv})}{(1-\sin\phi'_{peak}\sin\phi'_{cv})}$$

where $\phi'_{cv} = 31^0$; b and K_0 vary with depth and are shown in Figure 19.

Journal of Geotechnical and Geoenvironmental Engineering. Submitted June 16, 2009; accepted February 2, 2011; posted ahead of print February 3, 2011. doi:10.1061/(ASCE)GT.1943-5606.0000518

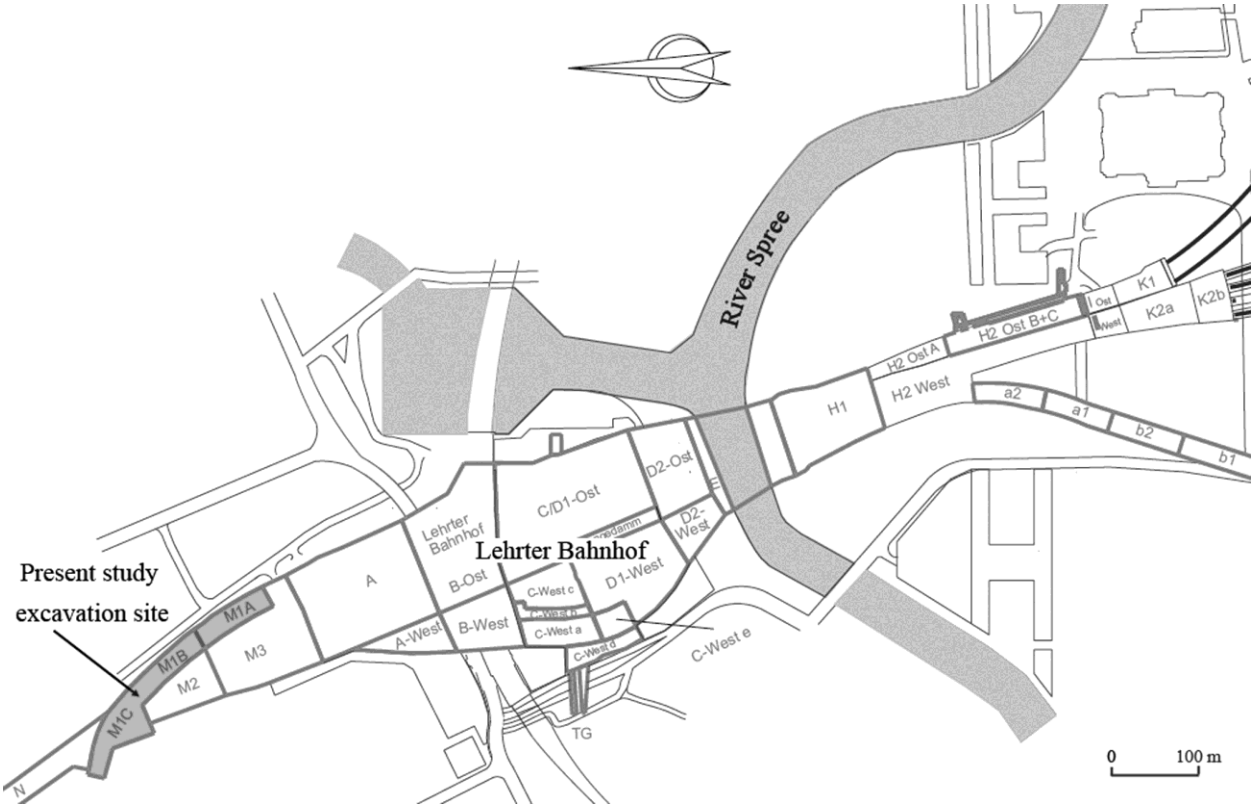

Figure 1: Excavation pits for the VZB project in Berlin (partial plan showing area north of Spree river)

Journal of Geotechnical and Geoenvironmental Engineering. Submitted June 16, 2009; accepted February 2, 2011; posted ahead of print February 3, 2011. doi:10.1061/(ASCE)GT.1943-5606.0000518

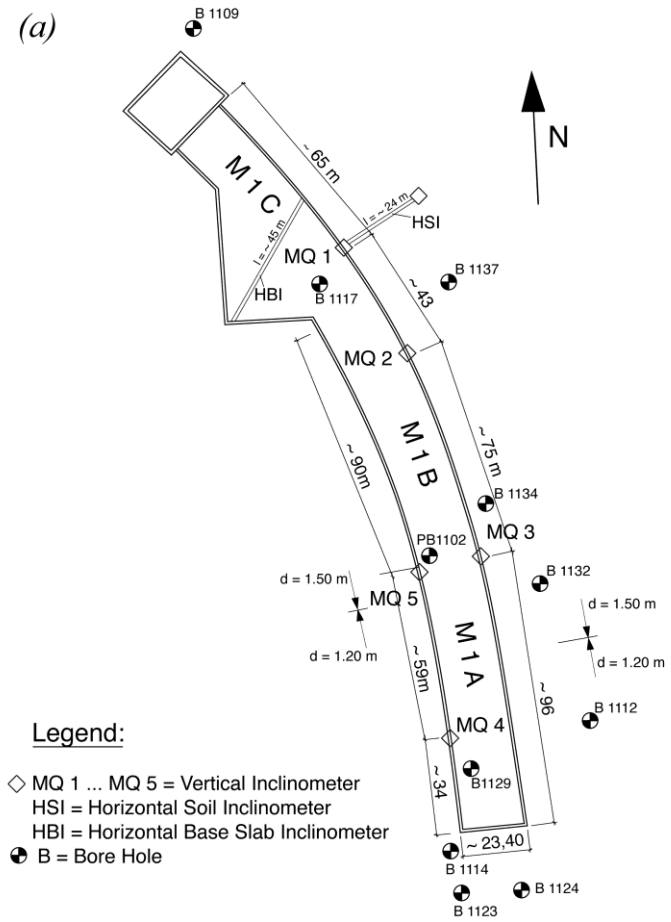

Figure 2a: Site plan with instrumentation and borehole locations

Journal of Geotechnical and Geoenvironmental Engineering. Submitted June 16, 2009; accepted February 2, 2011; posted ahead of print February 3, 2011. doi:10.1061/(ASCE)GT.1943-5606.0000518

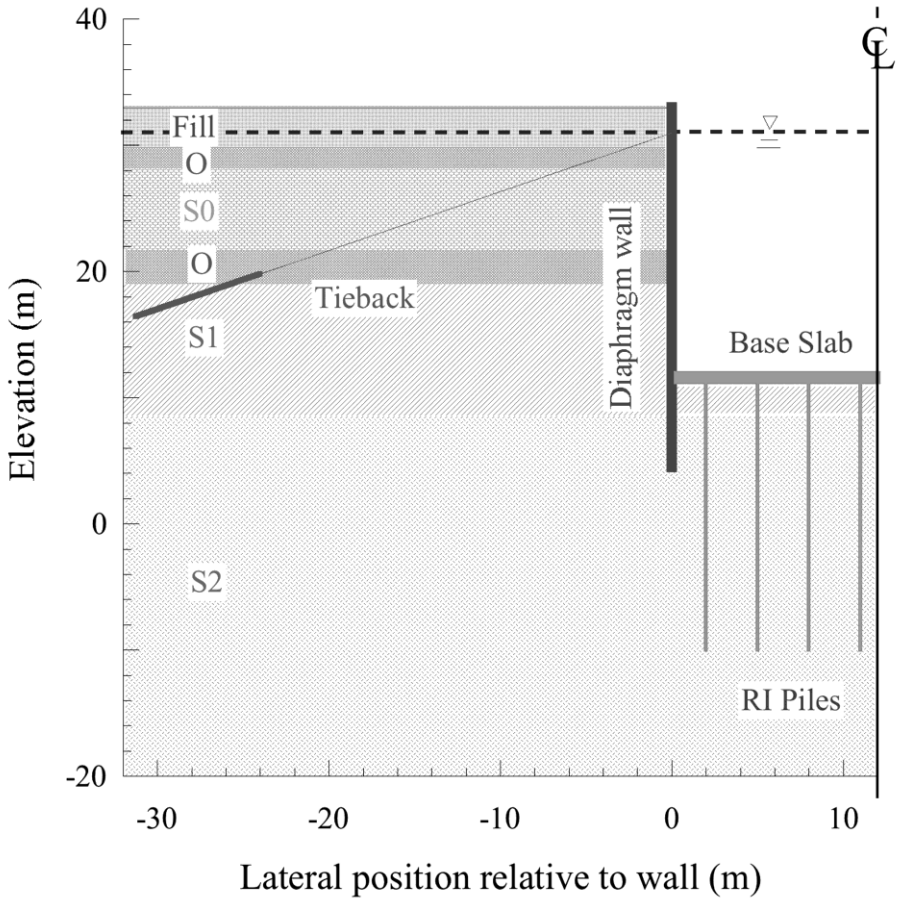

Figure 2b: Typical vertical section with lateral earth support system. Particular details for each cross section are summarized in Table 3 and are plotted to scale in the corresponding Figures 13-19.

Figure 2: Site conditions and excavation support system at M1 pit

Journal of Geotechnical and Geoenvironmental Engineering. Submitted June 16, 2009; accepted February 2, 2011; posted ahead of print February 3, 2011. doi:10.1061/(ASCE)GT.1943-5606.0000518

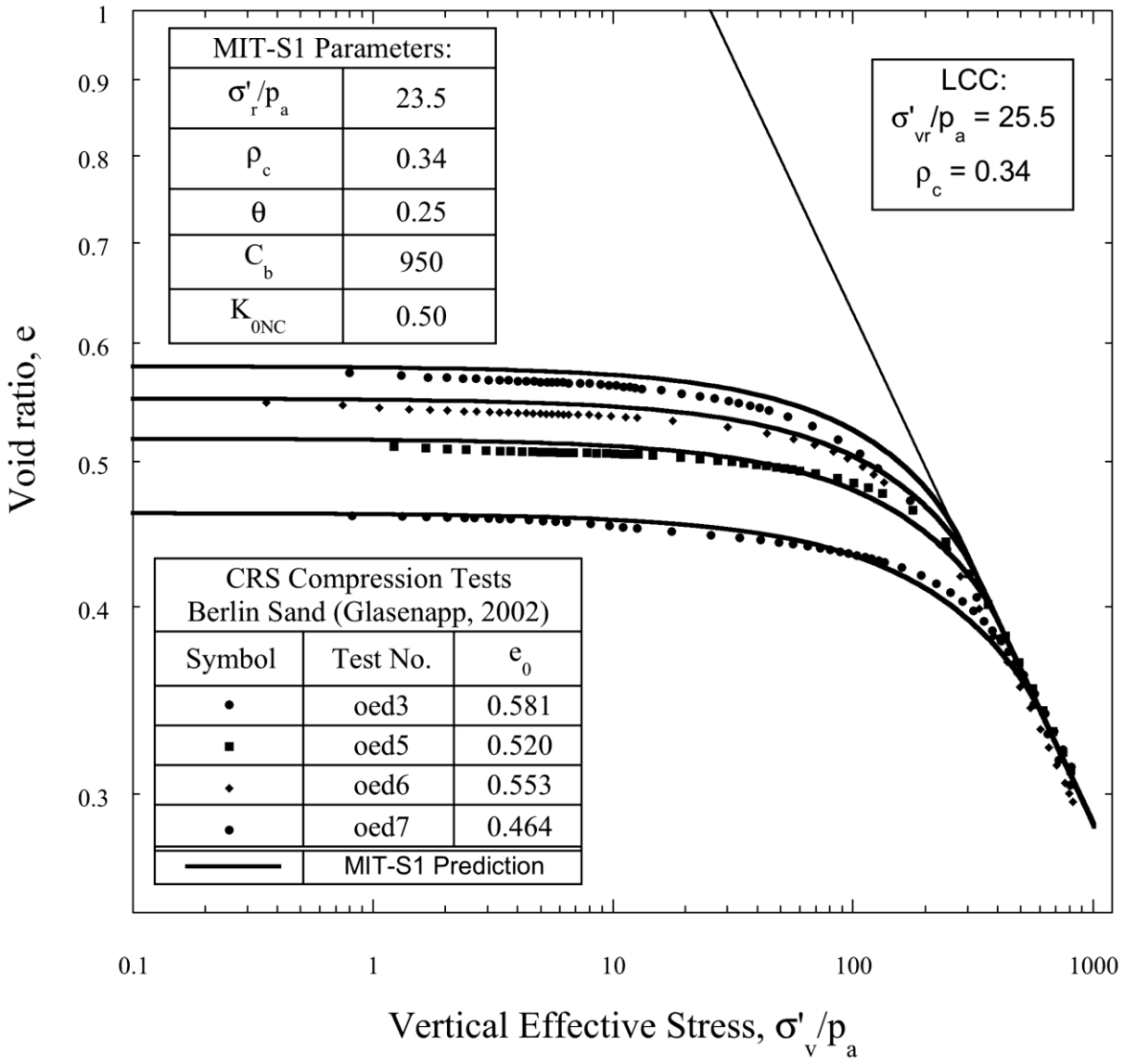

Figure 3: Comparison of predicted and measured 1-D compression behavior of Berlin sand

Journal of Geotechnical and Geoenvironmental Engineering. Submitted June 16, 2009; accepted February 2, 2011; posted ahead of print February 3, 2011. doi:10.1061/(ASCE)GT.1943-5606.0000518

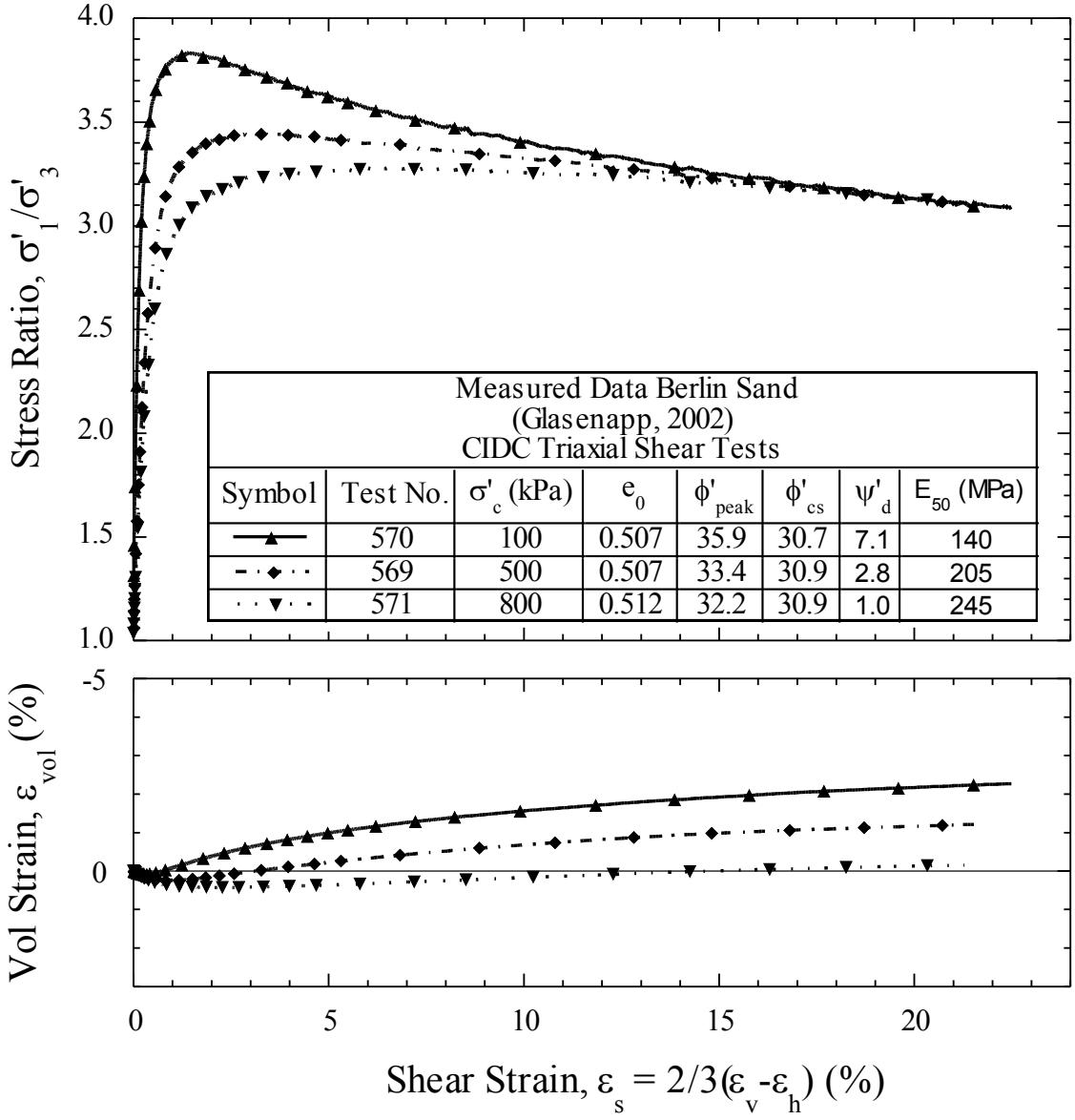

Figure 4: Effect of confining pressure on drained shear behavior of Berlin sand

Journal of Geotechnical and Geoenvironmental Engineering. Submitted June 16, 2009; accepted February 2, 2011; posted ahead of print February 3, 2011. doi:10.1061/(ASCE)GT.1943-5606.0000518

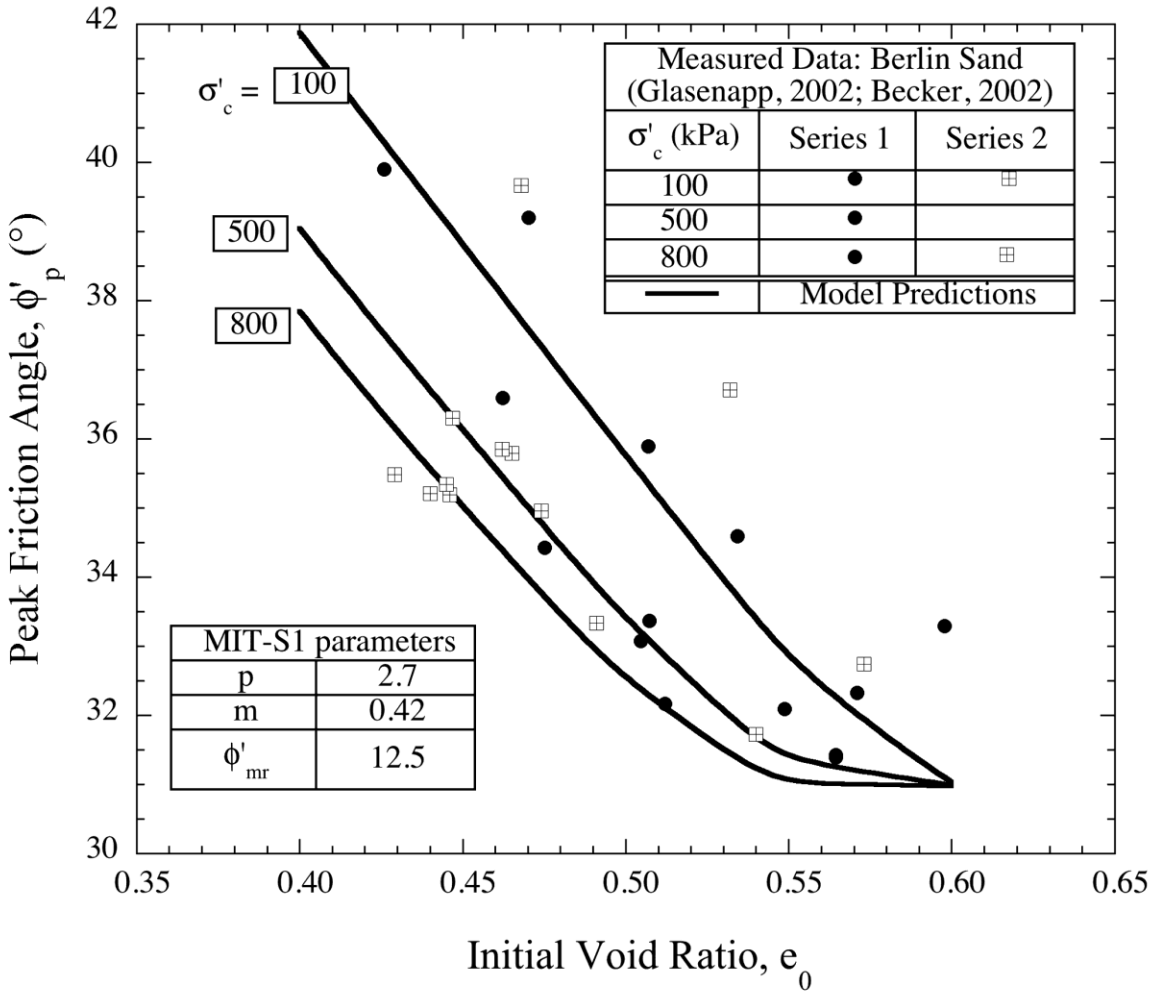

Figure 5: Comparison of predicted and measured peak friction angles in drained triaxial shear tests (CIDC) on Berlin sand

Journal of Geotechnical and Geoenvironmental Engineering. Submitted June 16, 2009; accepted February 2, 2011; posted ahead of print February 3, 2011. doi:10.1061/(ASCE)GT.1943-5606.0000518

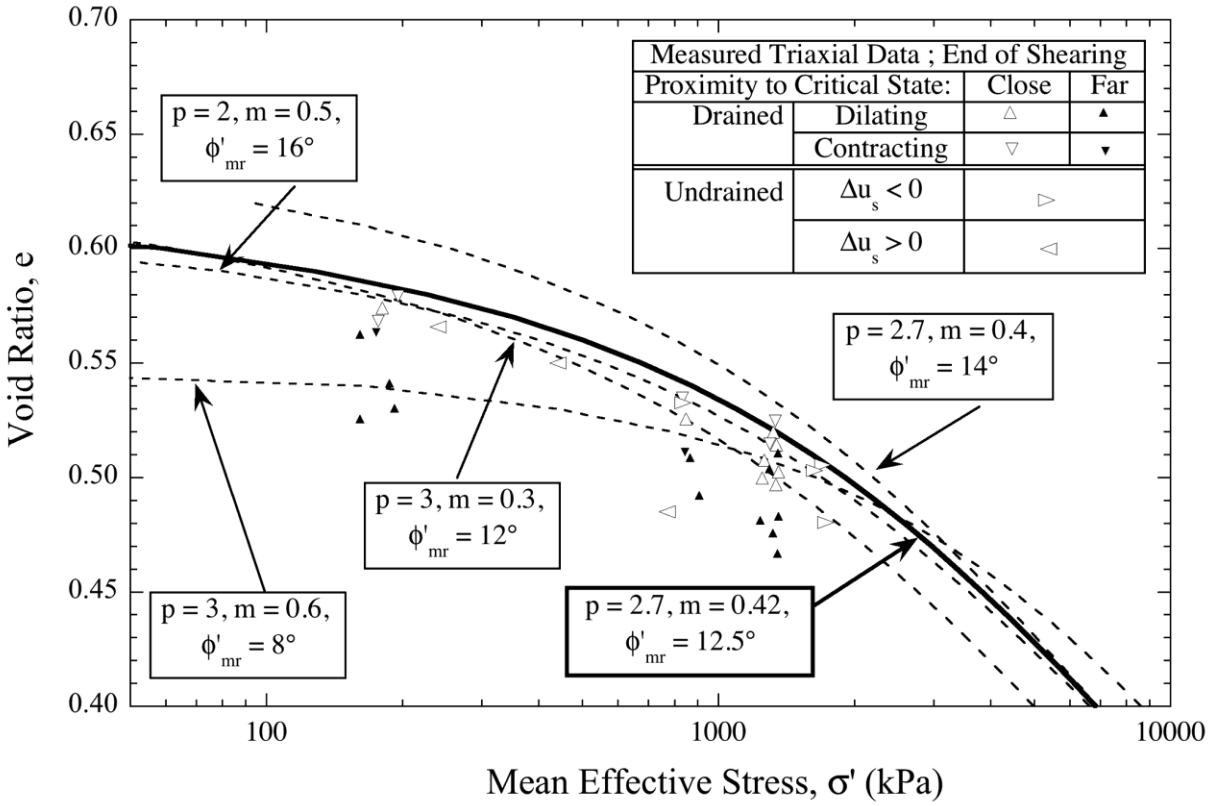

Figure 6: Interpretation of critical state conditions from triaxial shear tests on Berlin sand

Journal of Geotechnical and Geoenvironmental Engineering. Submitted June 16, 2009; accepted February 2, 2011; posted ahead of print February 3, 2011. doi:10.1061/(ASCE)GT.1943-5606.0000518

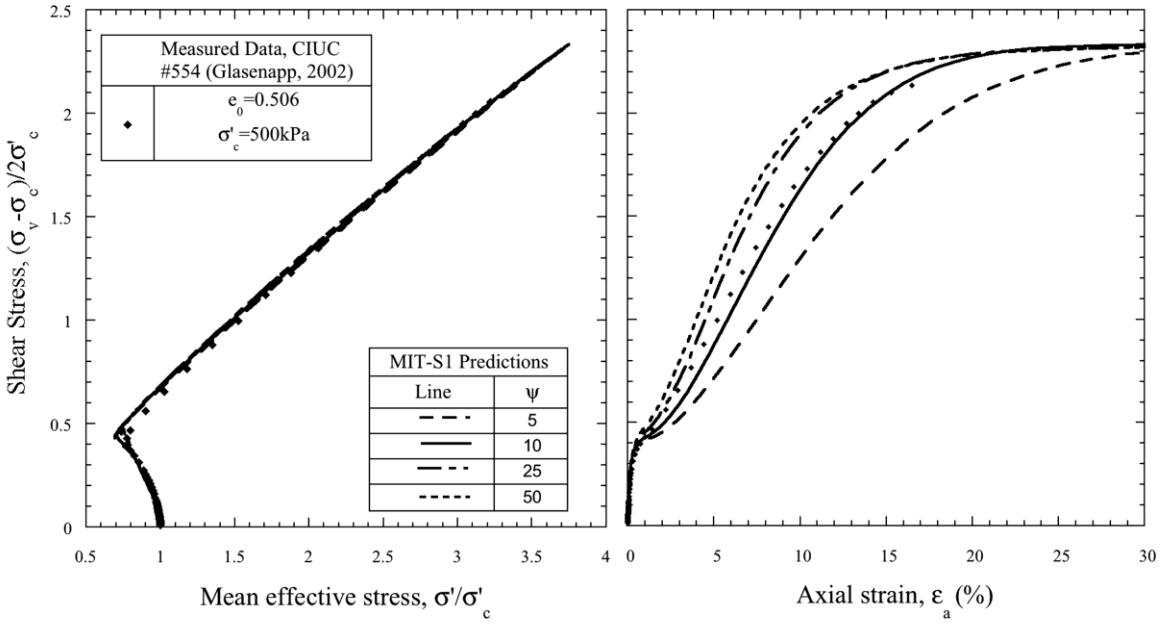

Figure 7: Calibration of parameter ψ from undrained shear test (ω_s = 4.0; Table 2)

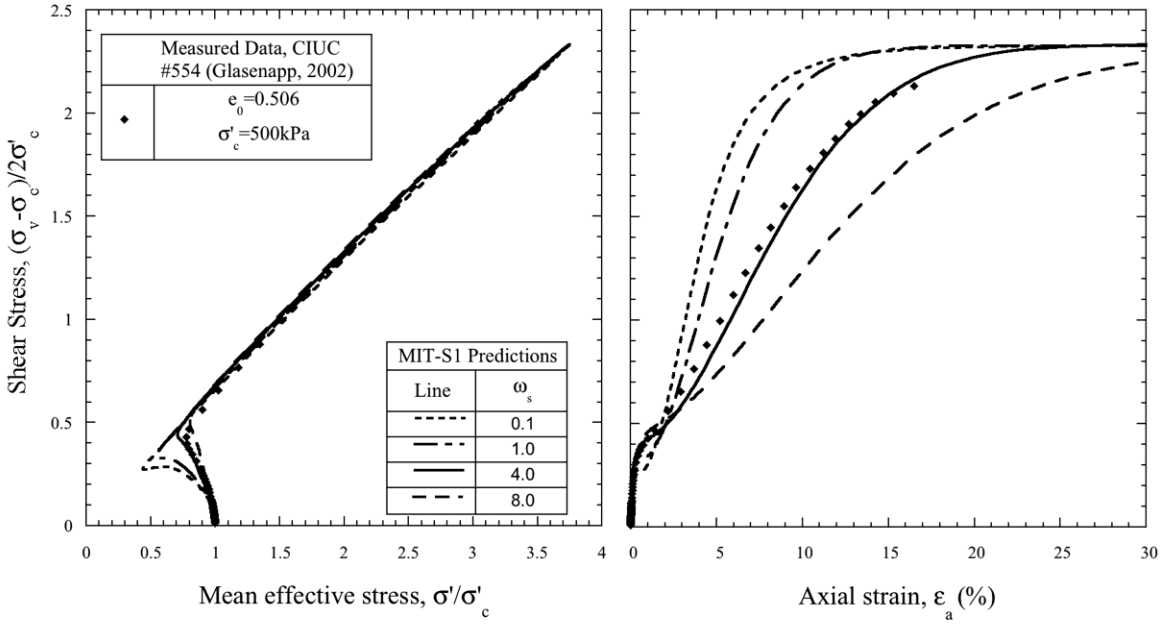

Figure 8: Influence of parameter ω_s on predicted undrained shear behavior (ψ = 10; Table 2)

Journal of Geotechnical and Geoenvironmental Engineering. Submitted June 16, 2009; accepted February 2, 2011; posted ahead of print February 3, 2011. doi:10.1061/(ASCE)GT.1943-5606.0000518

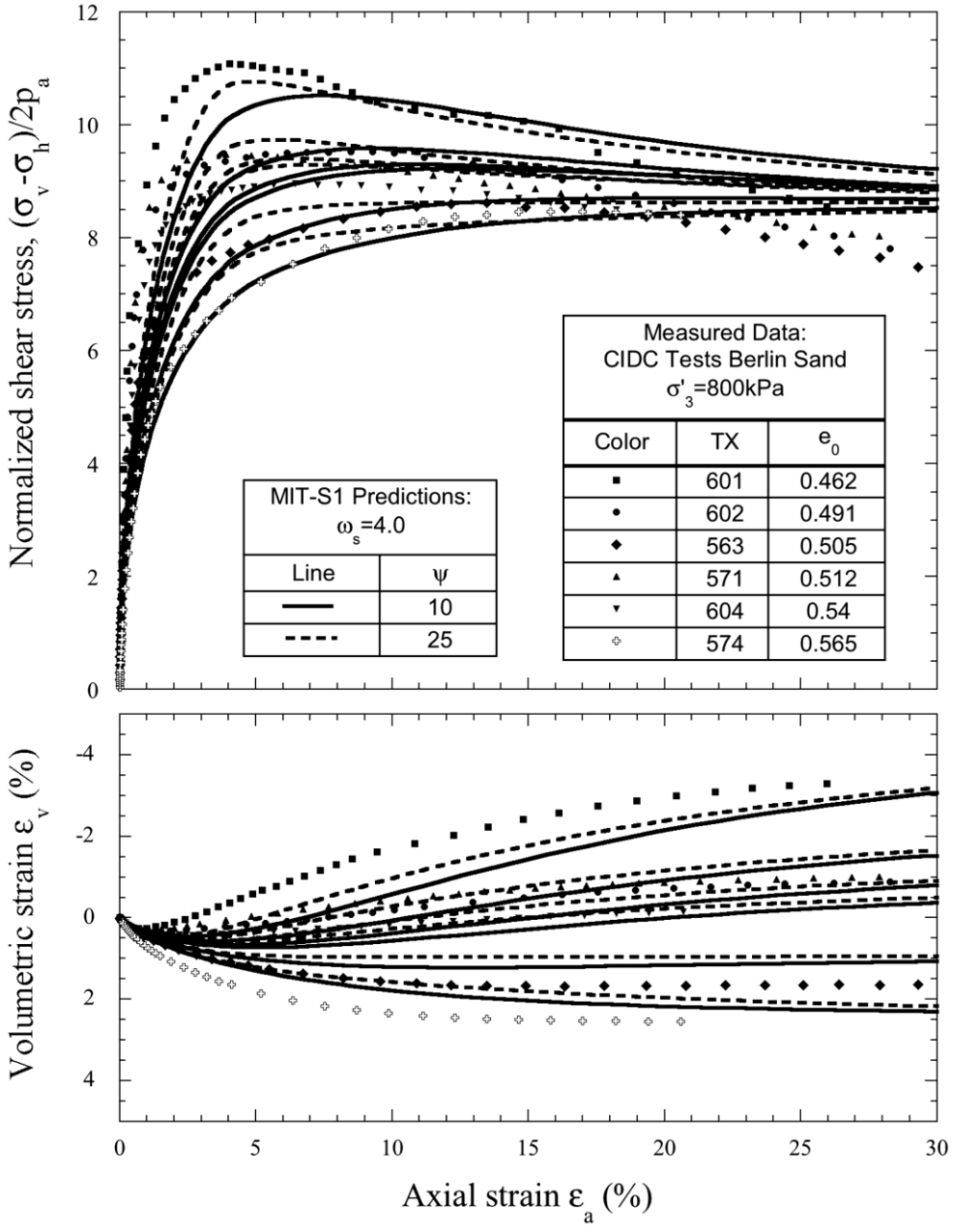

Figure 9: Effect of parameter ψ on MIT-S1 model predictions of drained triaxial shear tests (CIDC) on Berlin sand

Journal of Geotechnical and Geoenvironmental Engineering. Submitted June 16, 2009; accepted February 2, 2011; posted ahead of print February 3, 2011. doi:10.1061/(ASCE)GT.1943-5606.0000518

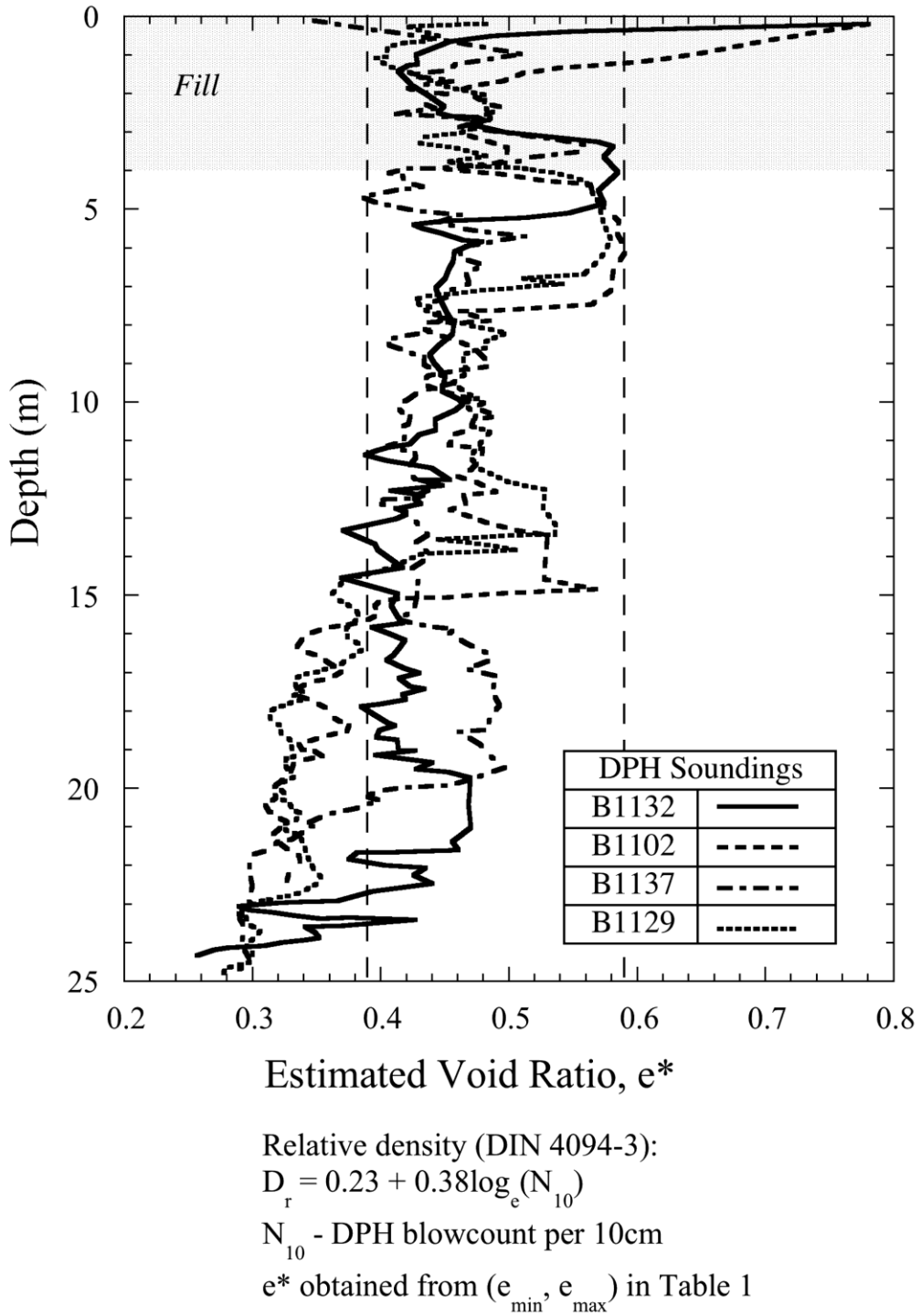

Figure 10: Estimated void ratio profile for M1 excavation

Journal of Geotechnical and Geoenvironmental Engineering. Submitted June 16, 2009; accepted February 2, 2011; posted ahead of print February 3, 2011. doi:10.1061/(ASCE)GT.1943-5606.0000518

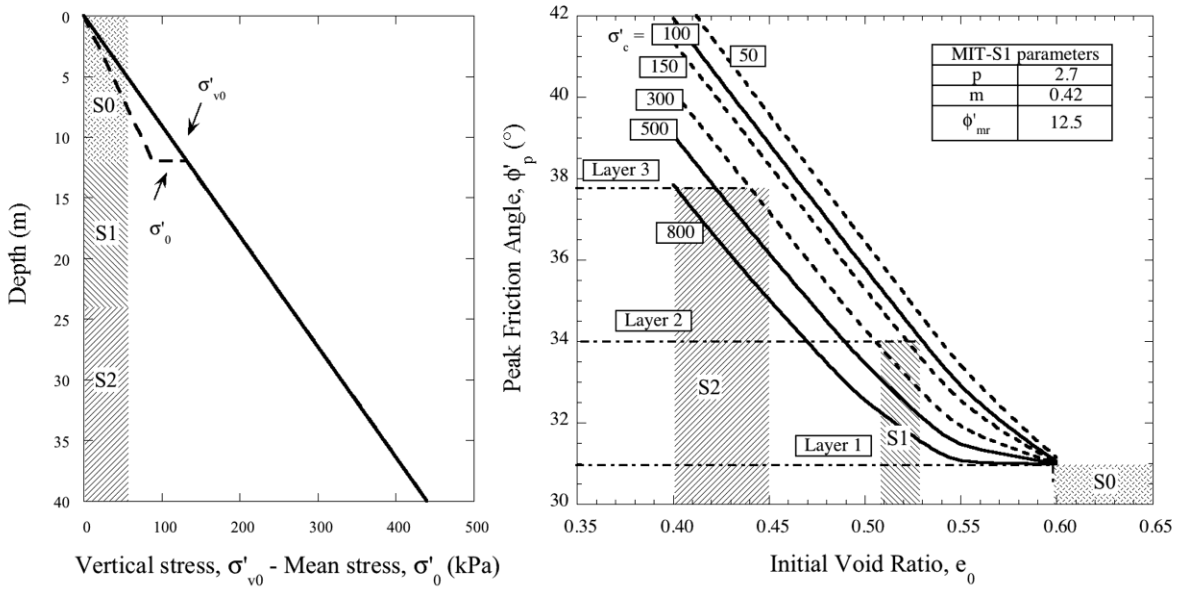

Figure 11: Selection of initial void ratio values for the 3-layered profile using the predicted peak friction angles from the calibrated MIT-S1 model

Journal of Geotechnical and Geoenvironmental Engineering. Submitted June 16, 2009; accepted February 2, 2011; posted ahead of print February 3, 2011. doi:10.1061/(ASCE)GT.1943-5606.0000518

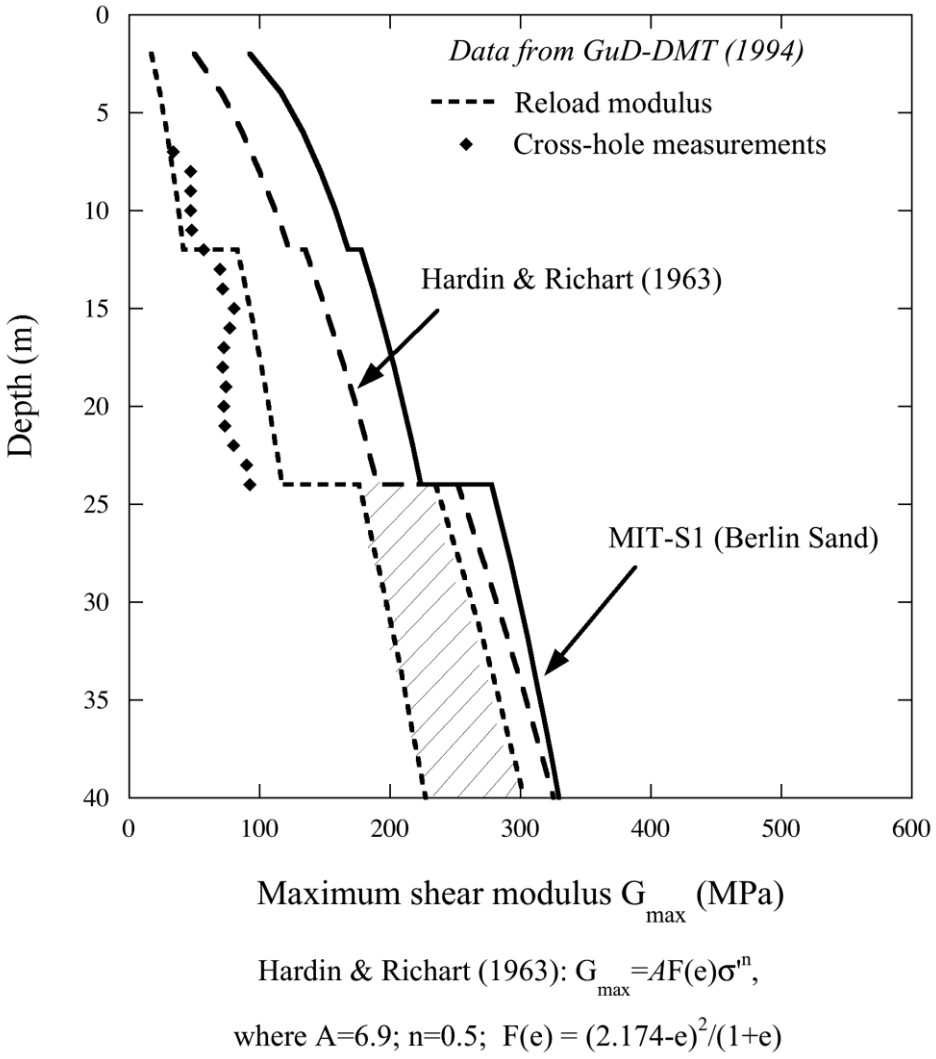

Figure 12: Maximum shear modulus profiles over depth.

Journal of Geotechnical and Geoenvironmental Engineering. Submitted June 16, 2009; accepted February 2, 2011; posted ahead of print February 3, 2011. doi:10.1061/(ASCE)GT.1943-5606.0000518

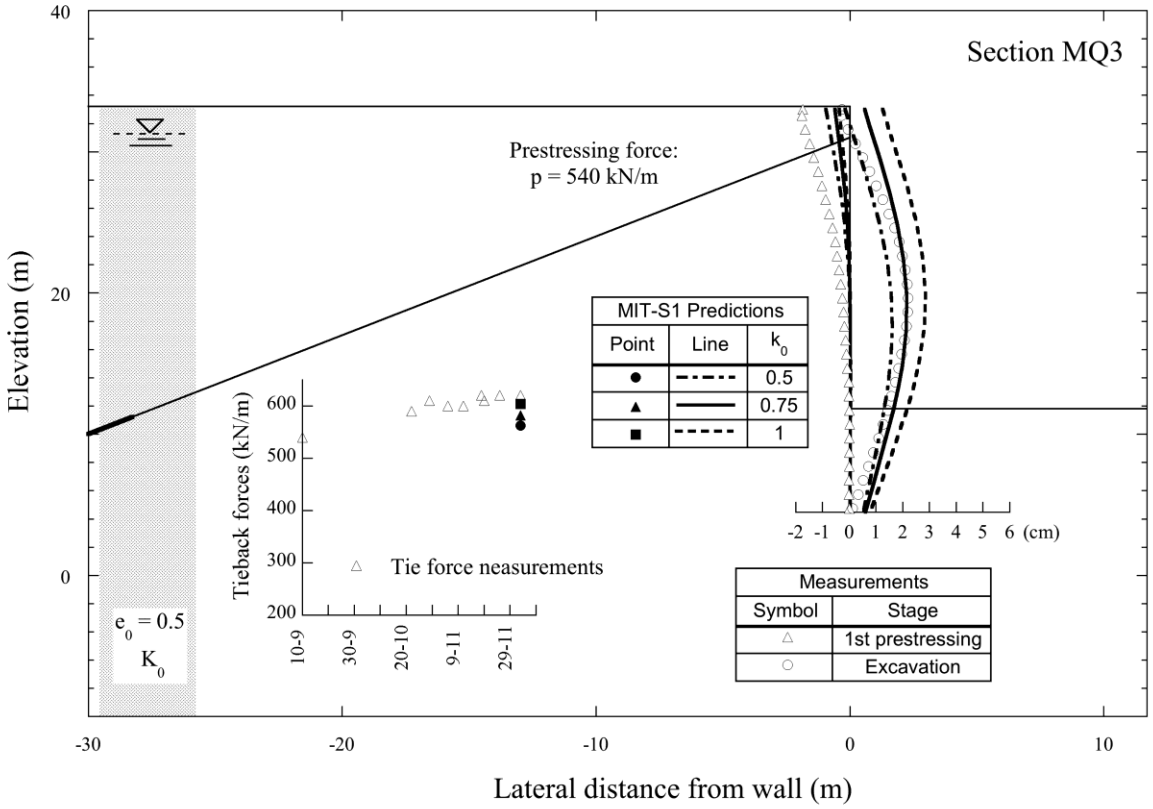

Figure 13: Effect of in-situ K_0 on lateral wall movements and tieback forces at MQ3

Journal of Geotechnical and Geoenvironmental Engineering. Submitted June 16, 2009; accepted February 2, 2011; posted ahead of print February 3, 2011. doi:10.1061/(ASCE)GT.1943-5606.0000518

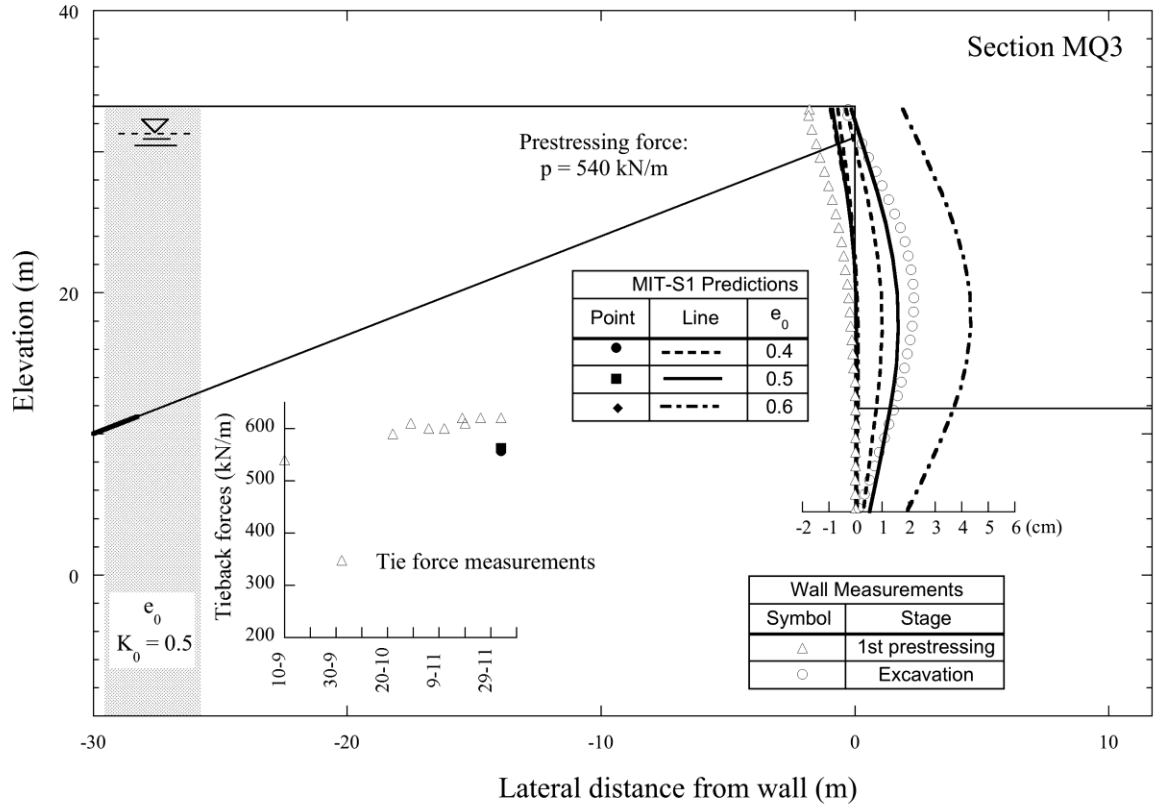

Figure 14: Effect of in-situ void ratio on lateral wall movements and tieback forces at MQ3

Journal of Geotechnical and Geoenvironmental Engineering. Submitted June 16, 2009; accepted February 2, 2011; posted ahead of print February 3, 2011. doi:10.1061/(ASCE)GT.1943-5606.0000518

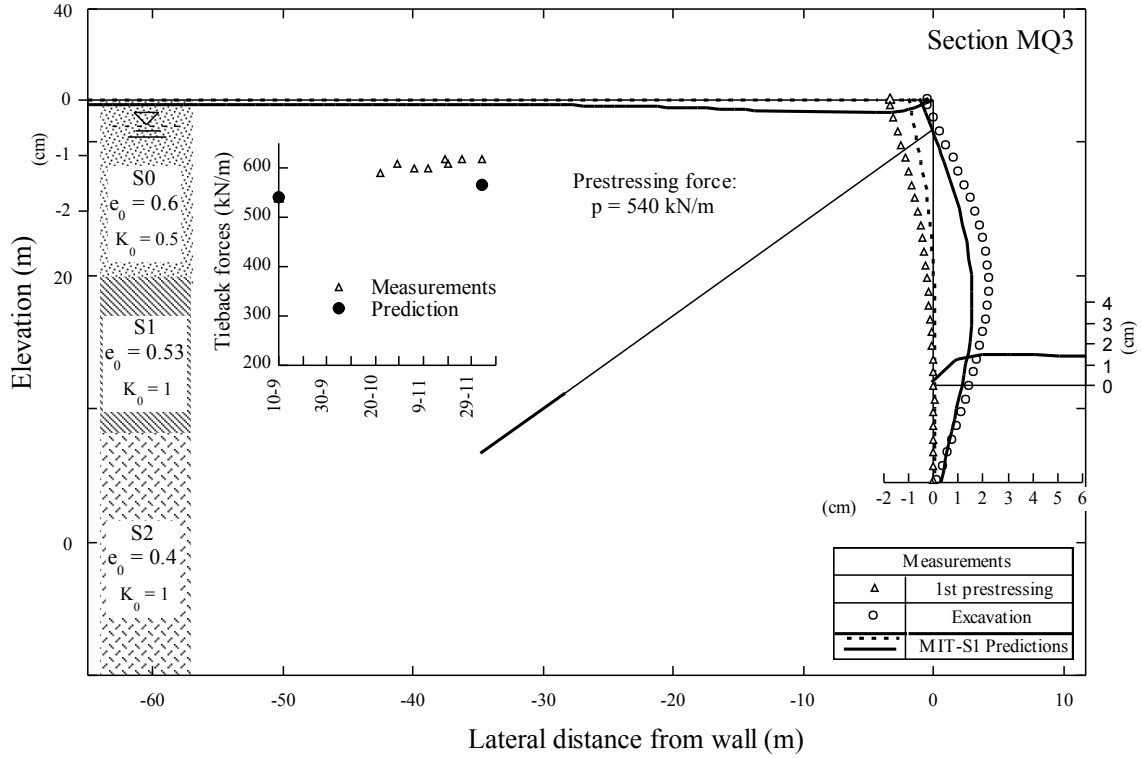

Figure 15: Predicted excavation performance for section MQ3 based on best estimate of state parameters

Journal of Geotechnical and Geoenvironmental Engineering. Submitted June 16, 2009; accepted February 2, 2011; posted ahead of print February 3, 2011. doi:10.1061/(ASCE)GT.1943-5606.0000518

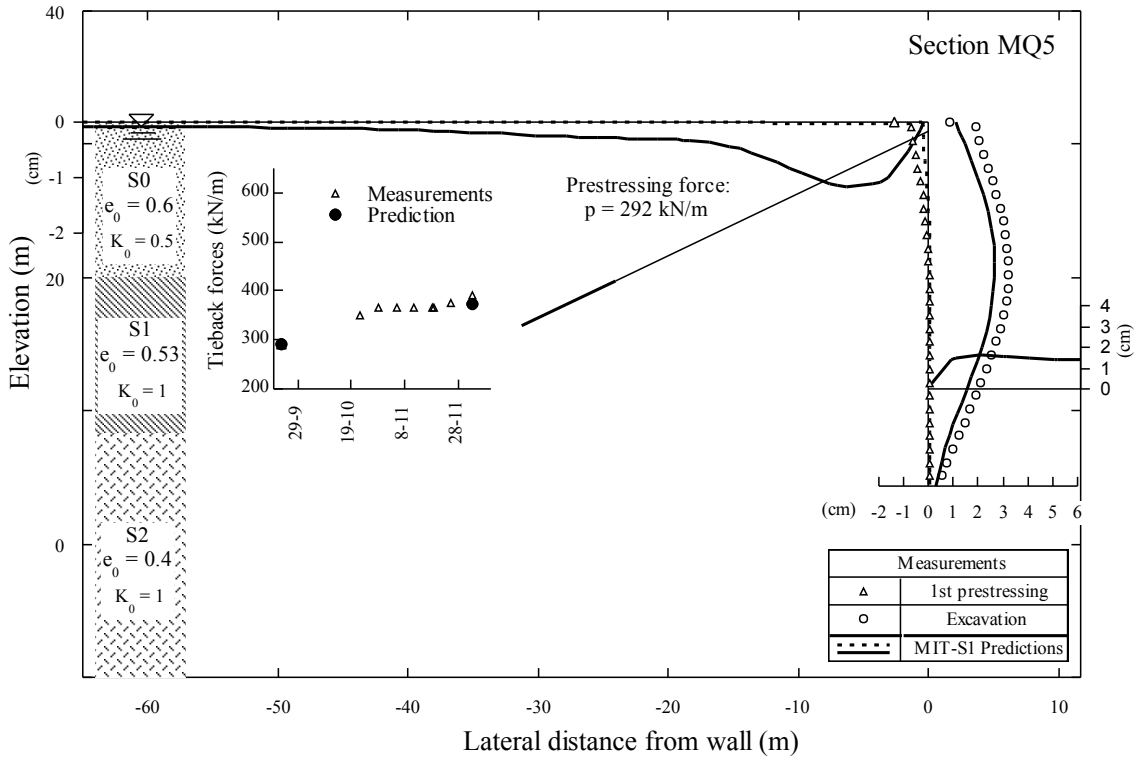

Figure16: Predicted excavation performance for section MQ5

Journal of Geotechnical and Geoenvironmental Engineering. Submitted June 16, 2009; accepted February 2, 2011; posted ahead of print February 3, 2011. doi:10.1061/(ASCE)GT.1943-5606.0000518

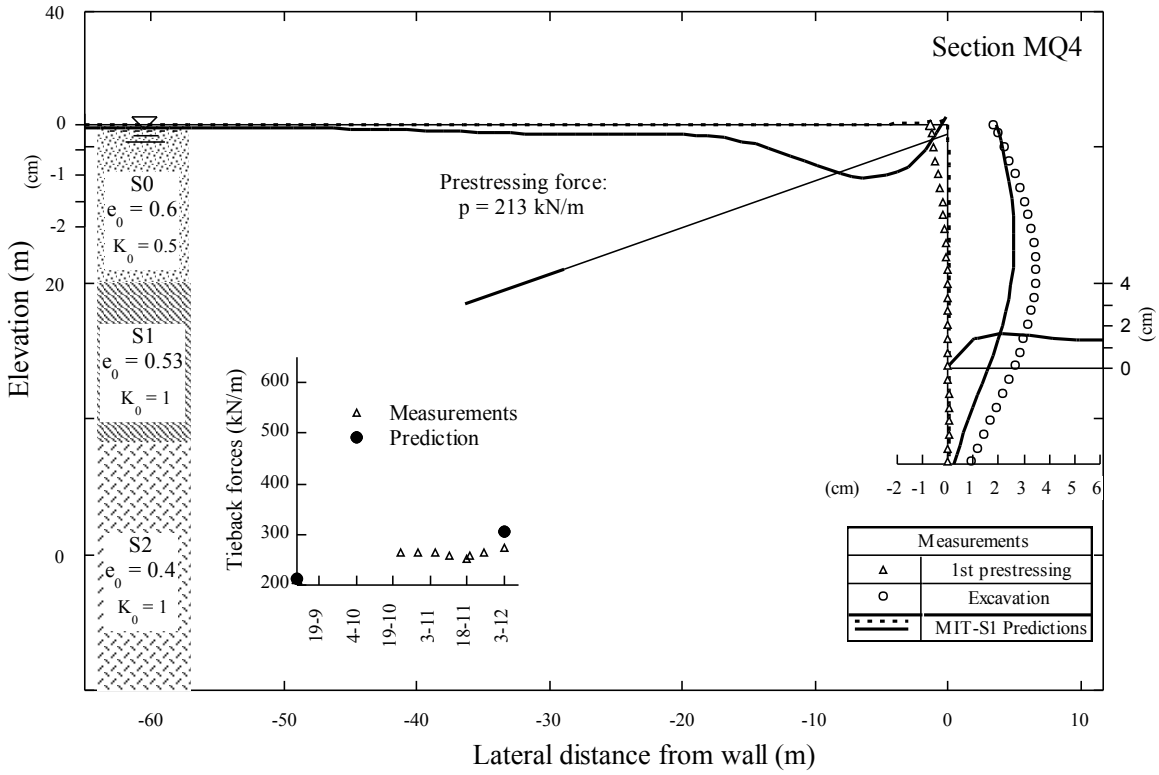

Figure 17: Predicted excavation performance for section MQ4

Journal of Geotechnical and Geoenvironmental Engineering. Submitted June 16, 2009; accepted February 2, 2011; posted ahead of print February 3, 2011. doi:10.1061/(ASCE)GT.1943-5606.0000518

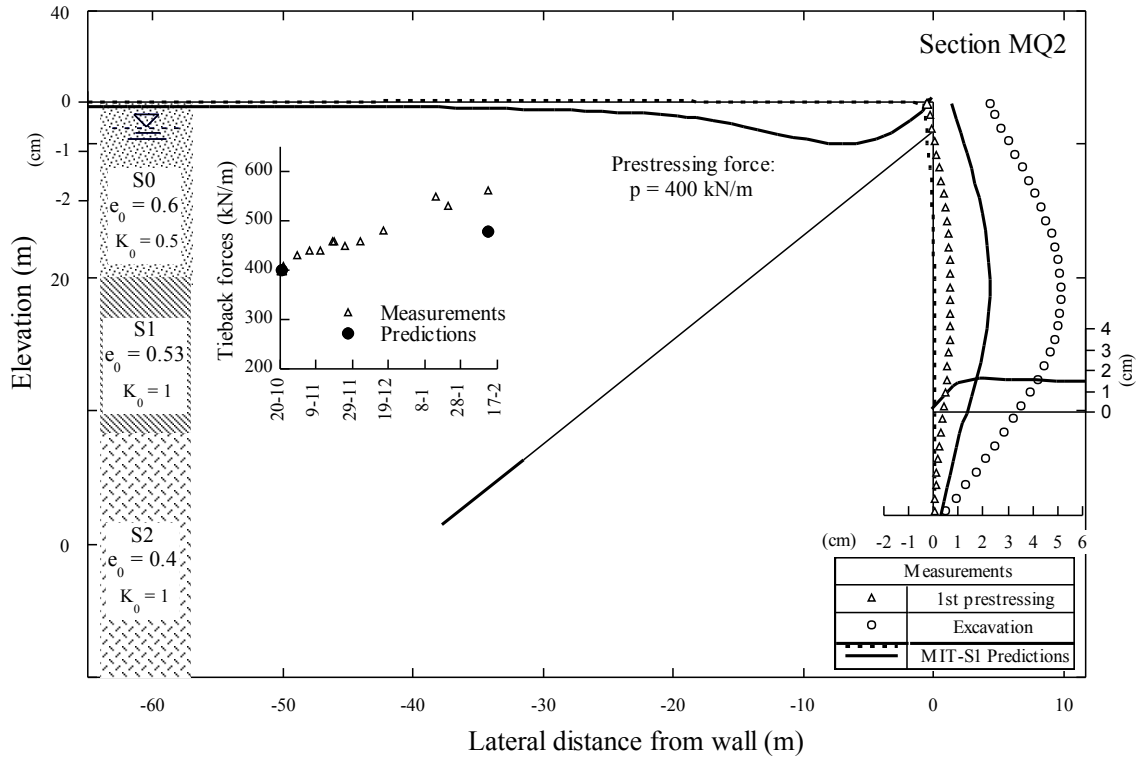

Figure 18: Predicted excavation performance for section MQ2

Journal of Geotechnical and Geoenvironmental Engineering. Submitted June 16, 2009; accepted February 2, 2011; posted ahead of print February 3, 2011. doi:10.1061/(ASCE)GT.1943-5606.0000518

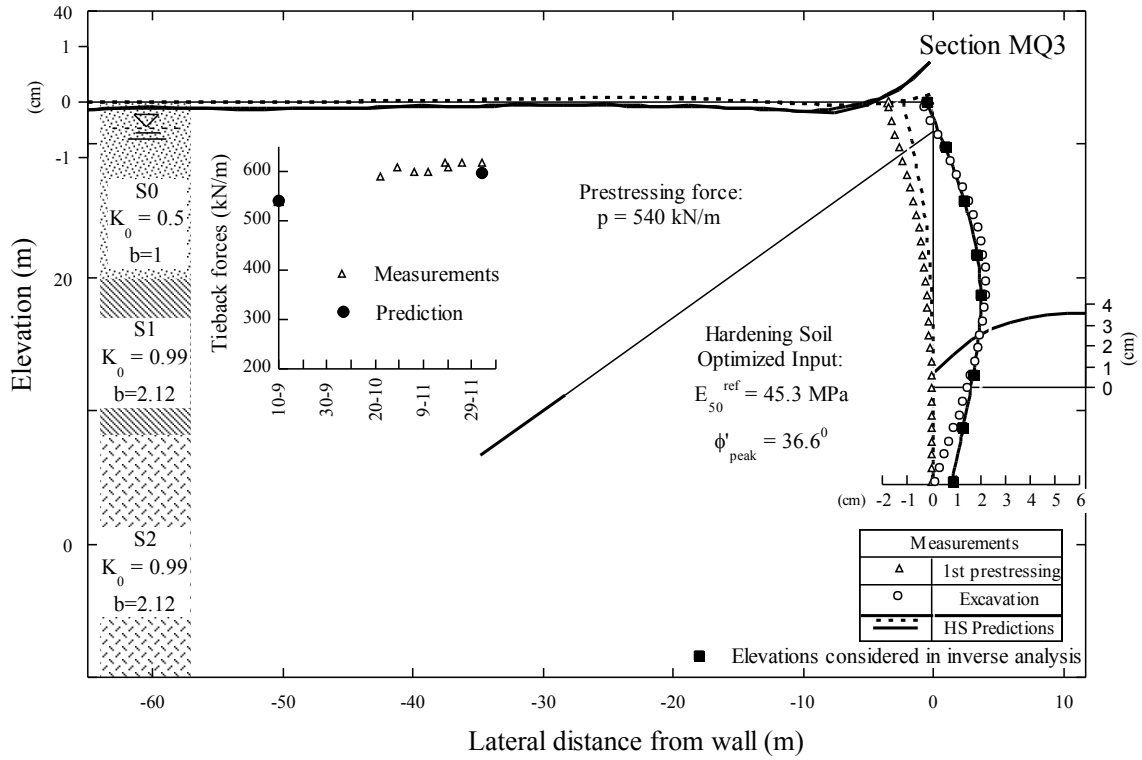

Figure 19: Predicted excavation performance for section MQ3 using the Hardening Soil Model. The input was optimized using genetic algorithms (Table 4).

Journal of Geotechnical and Geoenvironmental Engineering. Submitted June 16, 2009; accepted February 2, 2011; posted ahead of print February 3, 2011. doi:10.1061/(ASCE)GT.1943-5606.0000518

FIGURE CAPTIONS

Figure 1: Excavation pits for the VZB project in Berlin (partial plan showing area north of Spree river)

Figure 2a: Site plan with instrumentation and borehole locations

Figure 2b: Typical vertical section with lateral earth support system. Particular details for each cross section are summarized in Table 3 and are plotted to scale in the corresponding Figures 13-19.

Figure 2: Site conditions and excavation support system at M1 pit

Figure 3: Comparison of predicted and measured 1-D compression behavior of Berlin sand

Figure 4: Effect of confining pressure on drained shear behavior of Berlin sand

Figure 5: Comparison of predicted and measured peak friction angles in drained triaxial shear tests (CIDC) on Berlin sand

Figure 6: Interpretation of critical state conditions from triaxial shear tests on Berlin sand

Figure 7: Calibration of parameter ψ from undrained shear test (ω_s = 4.0; Table 2)

Figure 8: Influence of parameter ω_s on predicted undrained shear behavior (ψ = 10; Table 2)

Figure 9: Effect of parameter ψ on MIT-S1 model predictions of drained triaxial shear tests (CIDC) on Berlin sand

Figure 10: Estimated void ratio profile for M1 excavation

Journal of Geotechnical and Geoenvironmental Engineering. Submitted June 16, 2009; accepted February 2, 2011; posted ahead of print February 3, 2011. doi:10.1061/(ASCE)GT.1943-5606.0000518